# PREPARATION AND CHARACTERIZATION OF MICROSIZE Fe DOPED RGO/PVDF PIEZOELECTRIC MATERIAL: A SMART APPROACH FOR ENERGY HARVESTING

*A Major Project report submitted towards the partial fulfillment of the requirement for the award of the degree of*

**MASTER OF TECHNOLOGY**
**IN**
**POLYMER TECHNOLOGY**


*Submitted by*
**Tarun Kataria (2K14/PTE/11)**


*Under the Supervision of*


Dr. D. Kumar (Professor)

Dr. Jay Singh

DEPARTMENT OF APPLIED CHEMISTRY AND POLYMER TECHNOLOGY
DELHI TECHNOLOGICAL UNIVERSITY
DELHI-110042, INDIA

# CERTIFICATE

This is to certify that the M.Tech major project thesis entitled **"Preparation and characterization of microsize Fe doped RGO/PVDF piezoelectric material: A smart approach for energy harvesting"** submitted by Mr. Tarun Kataria to the Delhi Technological University, for the award of the degree of "Master of Technology" in Polymer Technology is a record of bonafide work carried out by him. Mr. Tarun has worked under our guidance and supervision and fulfilled the requirements for the submission of the thesis. The project work has been carried out during the session 2015-2016.

To the best of our knowledge and belief the content therein is his original work and has not been submitted to any other university or institute for the award of any degree or diploma.

Supervisor

Dr. Jay Singh & Dr. D. Kumar

# ACKNOWLEDGEMENT

First of all, I am grateful to the God for the good health and wellbeing that were necessary to complete this project.

I wish to express my sincere thanks to Dr. Jay Singh for providing me with proper guidance and all the necessary facilities for the research.

I place on record, my sincere thank you to Dr. D. Kumar, for his continuous encouragement.

I am also grateful to Mr. Gaurav Rastogi (PhD Scholar), I am extremely thankful and indebted to him for sharing expertise, and sincere and valuable guidance and encouragement extended to me.

I take this opportunity to express gratitude to all of the Department faculty members for their help and support. I also thank my parents for the unceasing encouragement, support and attention.

I also place on record, my sense of gratitude to one and all, who directly or indirectly, have lent their hand in this venture.

# ABSTRACT

Piezoelectricity is an important property that can be used for generation of electricity from external mechanical force. One of the most widely used piezoelectric polymers for generation of electricity is PVDF. In this project the important properties of Polyvinylidene fluoride, graphene oxide and iron were utilized and an optimum composite was made for harvesting energy, PVDF for its high piezoelectric property, graphene for its conductivity and mechanical properties and iron dust for its high conductivity. The amount of RGO and Fe was varied till an optimum amount of energy was harvested. Finally an optimum voltage of 0.93V was obtained, which was further brought into use for illuminating a LED. The LED was gown with the help of charge and voltage amplifying circuit. Now, the same circuit could also be used for other low power electronic devises like buzzers, ear phones, etc.

# Contents

## LIST OF TABLES



## LIST OF FIGURES

# *CHAPTER 1*

# Introduction

Today, the world is going through a tough period. The population of the world is increasing rapidly whereas due to careless use by humans, the conventional resources are decreasing at a very fast rate. Therefore people are switching to non-conventional natural resources like hydro energy, thermal energy, etc. but their production comes with a cost. Hydropower plants like dams disturb the natural life cycle of the rivers and also affect the productivity of soil whereas thermal plants create lot of harmful gases, so there is an immediate need of finding an alternative way to produce energy in an eco-friendly way.[1]

Due to the growing population, energy crisis and global warming all around the world, development of cheap, renewable and green energy technique to fulfill the energy demand of the future generation is one of the most serious challenges that we face today. Now, there are different type of energy available in our environment, such as light energy, thermal energy and chemical energy but mechanical energy is present in most abundance, due to its availability anywhere and at any time.[2] Therefore, self-powered technology is the best way to overcome the energy crisis of the world where no battery is needed and no heavy machinery Over the past few years, Self powered piezoelectric devices with polaractive PVDF film have become a greater source of attraction due to PVDF's amazing electroactive properties, such as piezoelectricity, pyroelectricity and ferroelectricity with many harvesting applications.[3] Due to these properties, applications of PVDF have increased enormously in different fields such as sensors, actuators, non-volatile memories, nanogenerators, biomedical and energy harvesters.[3−6]

The remarkable progress in portable electronic devices, steady reduction of the operating voltage, size, weight of the devices, opens the prefeasibility for self-powered electronic devices. For the past 30 years, the energy was harvested from environmental noise, friction, etc. but now mechanical deformation has become of great interest due to its larger impact on the energy sectors.[7] A number of attempts have been taken to construct a self-powered piezoelectric energy harvesting devices by well grown inorganic nanomaterials and its polymeric composites. Several piezoelectric materials including ZnO,[7] $BaTiO_3$, [8] PZT,[9] $ZnSnO_3$ [10] and GaN[11] etc.. Although they possess much higher efficiency in energy conversion, but they are cost intensive, toxic and brittle in nature which is harassing the environmental condition.

Recently, similar application with triboelectric based material have been realized, but they have some limitations like low durability, low stability, industrial packaging problems in open environment because of humidity, and high output voltage that can damage the electronic circuitry which may produce sparks or even fire. [12,13] Polymer based piezoelectric material can overcome these limitations because they produce low voltage when applied with mechanical stress. Also, they are, biocompatible, environmentally stable, and flexible PVDF composites with easy preparative method and cost-effectiveness are some of its plus points.

The generation of piezoelectric polar polymorphic phases in the semi-crystalline thermoplastic PVDF polymer matrix is the main reason behind the piezoelectric energy harvesting property of PVDF. It is well known that, PVDF is the most favorable piezoelectric material due to its high piezoelectric co-efficient as compared to other currently available polymers, which are highly applicable to harvest electrical energy from the mechanical response, predominantly applicable in portable and low power electronic devices.[14] Moreover PVDF film, being very flexible and does not depolarize under high alternating electric field due to its excellent stabilization over a long period of time.[15] The piezoelectric properties of PVDF are mainly observed for its β and γ-crystalline polar phases.[16]

PVDF has four types of phases viz., α, β, γ and δ, which are represented by stereo-chemical representation of the structures with alternating s-gauche and s-trans carbon-carbon bonds such as TGTḠ, T3GT3Ḡ, TTTT, and TGTḠ (polar) (T = trans, G = gauche +, $\bar{G}$ = gauche –), respectively. Among the four phases, β/γ-phase mainly shows valuable piezoelectric property.[17] In addition, the delayed saturation of polarization even at high external electric field enables the γ-phase to exhibit high energy density with high energy storage capacity.[18,19] The γ-phase of PVDF also shows superior piezoelectric coefficient, although the latter one being more polar.[20,21] Furthermore, the γ-phase of PVDF is more environmentally stable as compared to the β-phase due to its higher melting temperature which restricts the gradual decaying of the polar phases, making it more suitable for production of thermally stable and long-lasting devices.[22] But, in order to use PVDF in piezoelectric energy harvesting application, the nucleation of γ and β-phases is a very essential parameter due to their polar electroactive formation.

Due to stable polar electroactive phases in PVDF, several processes like mechanical stretching under electric field by controlling pressure had been adopted, however, the main problem was that, the quantity of the films and batch production in industry are not up to the mark for the device production. So, the best alternative way was to add fillers into the PVDF matrix.

Recently, nanofillers were in focus to improve the functionalities of PVDF by stabilizing γ/β-polymorphology which was a very essential part to improve the piezoelectric energy harvesting efficiency of the PVDF based composites. Several research groups have attempted to increase the piezoelectric energy harvesting efficiency by stabilizing electroactive phases by combining PVDF with fillers such as graphene,[23] MWCNT,[24] CTAB,[25] graphene-CuS, [27] graphene-ZnO , [26] nanoclay, [28] PMMA-RGO,[29] and Ferrite.[30]

In this study, I report a new, flexible, low cost, light-weight Fe-doped RGO/PVDF (Fe-RGO/PVDF) composite piezoelectric material prepared through solution casting method.
Numerously, Fe-RGO/PVDF composites film showed high performances of piezosensivity under external repeating pressure where traditional electrical poling is avoided. Graphene and their derivatives have been chosen as conducting nanofiller due to its high surface area and aspect ratio, and superior mechanical, electrical and thermal properties.[31] In addition, Fe-RGO nanofillers have been used as an additive for the nucleation of the electroactive γ-phase in PVDF, it was possibly used for the production of flexible piezoelectric energy harvesting devices, as huge number of vertical compression scheme like in roads, shoes, bridges, footpaths, tires of vehicles, etc. could be utilized. Besides these properties it was expected that, this composite could be used as a tactile sensor and magneto electric material for data storage. [32]

The Fe-RGO/PVDF composite exhibited superior piezoelectric energy harvesting and ferroelectric property where higher proportion of polar piezoelectric γ-phase of PVDF was achieved simply by solvent casting method, which exclusively produced the output voltage of 1.0V. To the best of our knowledge, no work has been done for the γ-phase stabilization of PVDF applicable as piezoelectric energy harvesting material using Fe-RGO filler. Also, the touch sensitivity of an un-poled Fe-RGO/PVDF composite satisfied the great potential feasibility for development of smart sensors for next generation electronic devices.[32]

# *CHAPTER 2*

# Literature Review

## 2.1 Energy harvesting

Energy harvesting is a process by which suitable amount of energy can be derived from various external sources like wind energy, solar energy, thermal energy, etc. Energy harvesting devices provide a small amount of energy that is suitable for powering low power electronic devices. One great advantage of this process is that the energy source for these energy harvesters is free and unlimited.[33]

Energy harvesters converting ambient energy to electrical energy have attracted large interest in both military and commercial sectors. Some harvesters convert motion, such as that of ocean waves, into electric energy to be used by oceanographic monitoring sensors. Its future applications may include high power output devices to serve as reliable power stations for large systems. Other application is in electronics, where energy harvesting devices can power cellphones, computers, radio equipment, etc. [34]

There are number of energy harvesting materials that can be used to harvest energy from external sources. Some of them are

1. Photovoltaic
2. Photoelectric
3. Pyroelectric
4. Thermoelectric
5. Electrostatic
6. Tree based, etc.

## 2.2 Polyvinylidene fluoride (PVDF)

Piezoelectricity is the charge that gets accumulated in certain solid materials in response to applied external mechanical force. The word piezoelectricity means electricity generated from applying pressure. It was first discovered by the French physicists Pierre Currie and Jacques Currie in 1880.

Piezoelectric effect is an electromechanical interaction between mechanical and the electrical state in crystalline materials in a linear way with no inversion symmetry. Some of the piezoelectric materials known are certain ceramics, crystals, bones, DNA and various proteins etc. [35]

The piezoelectric effect is a reversible process in the materials that exhibit the direct piezoelectric effect (the internal generation of electrical charge which is a result of an applied mechanical force), they also exhibit the reverse piezoelectric effect (internal generation of a mechanical strain which is a result of an applied electrical field). For example, a lead zirconate titanate crystal generates some piezoelectricity when its static structure is deformed by 0.1% of the original dimension whereas; the crystal will change about 0.1% of its static dimension when an external electric field is applied to it. The energy generated because of external forces depends upon many factors like the rate of change of force, film composition, width of the film, environmental conditions, area on which the force is applied, etc.

Piezoelectricity is found in a number of useful applications, e.g. production and detection of sound, electronic frequency generation, microbalances, generation of high voltages, to drive an ultrasonic nozzle, and ultrafine focusing of assemblies. It is also the basic concept behind a number of scientific instrumental techniques having atomic resolution, everyday uses, such as an ignition source for lighters, push-start for propane barbecues, and quartz watches, the scanning probe microscopies, such as STM, MTA, AFM, etc.[36-37]

One of the most widely used piezoelectric polymer for generation of electricity is PVDF. PVDF stands for Polyvinylidene fluoride, which is a thermoplastic, semi-crystalline polymer with approximate degree of 50% crystallinity. Like other semicrystalline polymers, it consists of a lamellar structure with mixed amorphous regions. Its chemical structure contains repeating units of doubly fluorinated ethene $CF_2$–$CH_2$:

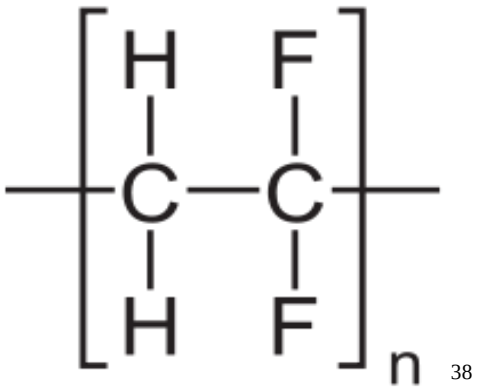

[38]

Figure 1: Chemical structure of PVDF

The film of PVDF is transparent in visible and near infrared region but it is absorptive in nature in the far infrared region of the electromagnetic spectrum. It melts at around 170°C and its density is 1780 kg/m$^3$(approximately). It is mechanically a durable and flexible material.

For piezoelectric applications, it is drawn, uniaxially or biaxially, many times of its length. Its elastic constant, also depends on this draw ratio. Therefore, if a film is drawn at 140°C to the ratio of 4:1, its modulus value would be 2.1 GPa, whereas PVDF film with draw ratio of 6.8:1, it would be 4.1 GPa. The resistivity of the PVDF film depends upon its stretch ratio. For example, for low stretch, the resistivity is approximately $6.3\times10^{15}\Omega$cm, whereas for high stretch ratio 7:1 it is $2\times10^{16}\Omega$cm. [23]

PVDF does not have a high piezoelectric coefficient as compared to other commonly used materials, like PZT or $BaTiO_3$. But, it has a unique property of not to get depolarized while subjected to a high alternating electric field which means that although the value of $d_{31}$ of PVDF is 10% of that of PZT, the maximum strain observable in PVDF film would be 10 times greater than in PZT, this is because the maximum permissible field for PVDF is 100 times greater. The film also exhibits good stability: When kept at 60°C, it slowly loses its sensitivity by about 2% over 6 months. [2]

Another advantage of a piezoelectric film over a piezo ceramic is its low acoustic impedance, which is about that of water, human tissue, and some other organic materials. For example, an acoustic impedance of a piezoelectric film is just 2.6 times that of water, but a piezoelectric ceramic is 11 times greater .A close impedance match helps greater transduction of acoustic signals in tissue and water.

Some important properties of the piezoelectric films are:

• It has wide frequency range: 0.001 Hz to 109 Hz

• It has vast dynamic range: 10−8–106 psi.

• It has low acoustic impedance: close to water, human tissue, and some adhesive systems

• It has high elastic compliance

• It has high voltage output: 10 times higher than piezoelectric ceramic film for the same input force.

• It has high dielectric strength: withstanding strong fields, where most piezoelectric ceramics depolarize.

• It has high mechanical strength and impact resistance.

• It has high stability of resisting moisture, most chemicals, oxidants, and nuclear and U.V. radiation

• It has can be fabricated into many shapes.

• It has can be glued with commercial adhesives

PVDF is also pyroelectric producing electrical charges in response to a change in temperature. PVDF also strongly absorbs infrared energy within 7–20-μm wavelength range, which covers the same wavelength spectrum as heat from our body.

## 2.3 PVDF working

The PVDF film works as a piezoelectric material which means when an external force is applied on it the molecules attached to the long chain of poly (vinylidene fluoride) polymer get aligned i.e. the hydrogen molecules move to one side and the fluoride molecules move to the other side which in turns creates dipoles and results in the generation of positive potential on one side of the film (due to hydrogen) and a negative potential to the other side of the film (due to high electronegativity of fluorine atoms) this leads to generation of a potential difference among the two opposite sides of the film, this leads to generation of charges and electrical energy is produced.[19]

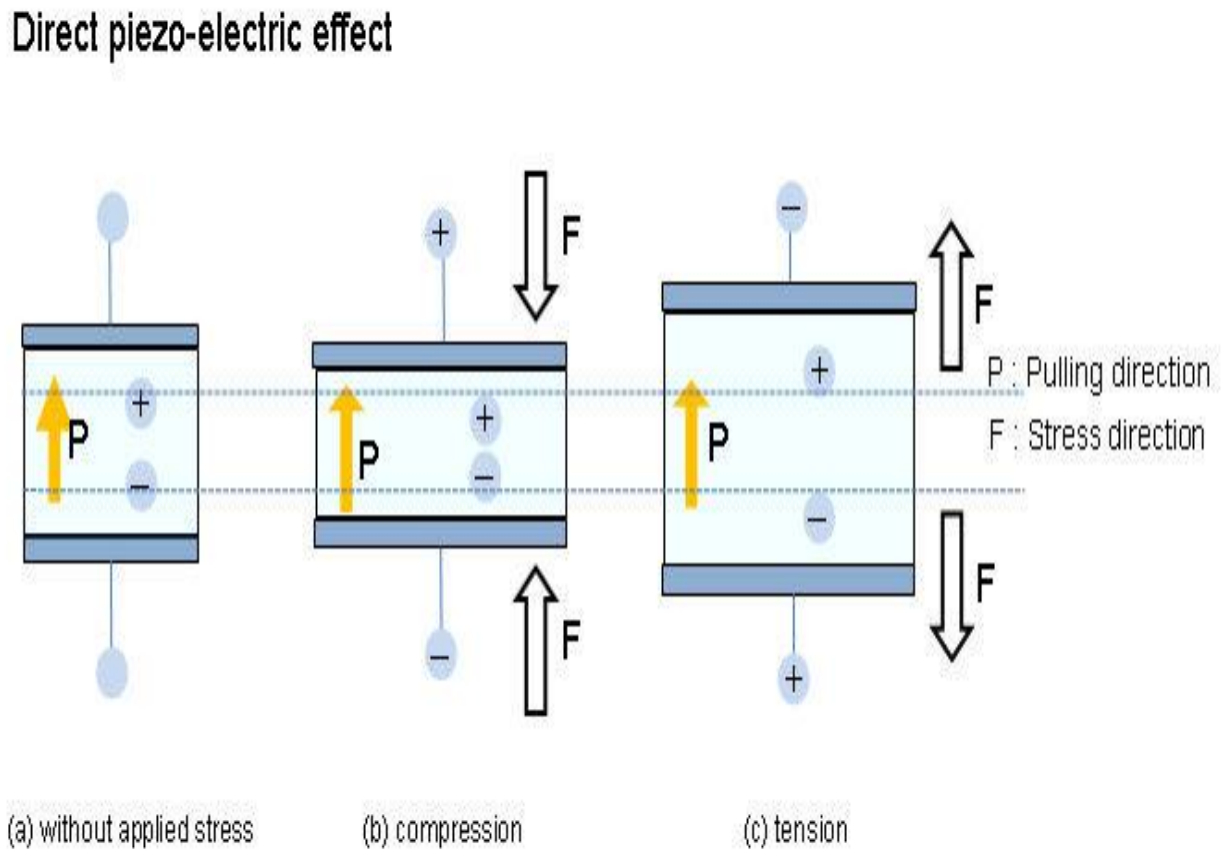


Figure 2: Working of PVDF when pressure is applied

The above figure shows the alignment of molecules when an external pressure is applied on the film. The alignment of H atoms on one side and F atoms on the other side creates a potential difference due the difference in their electro-negativities. This in turn helps in generation of charges and hence mechanical force is converted into electrical energy.[6]

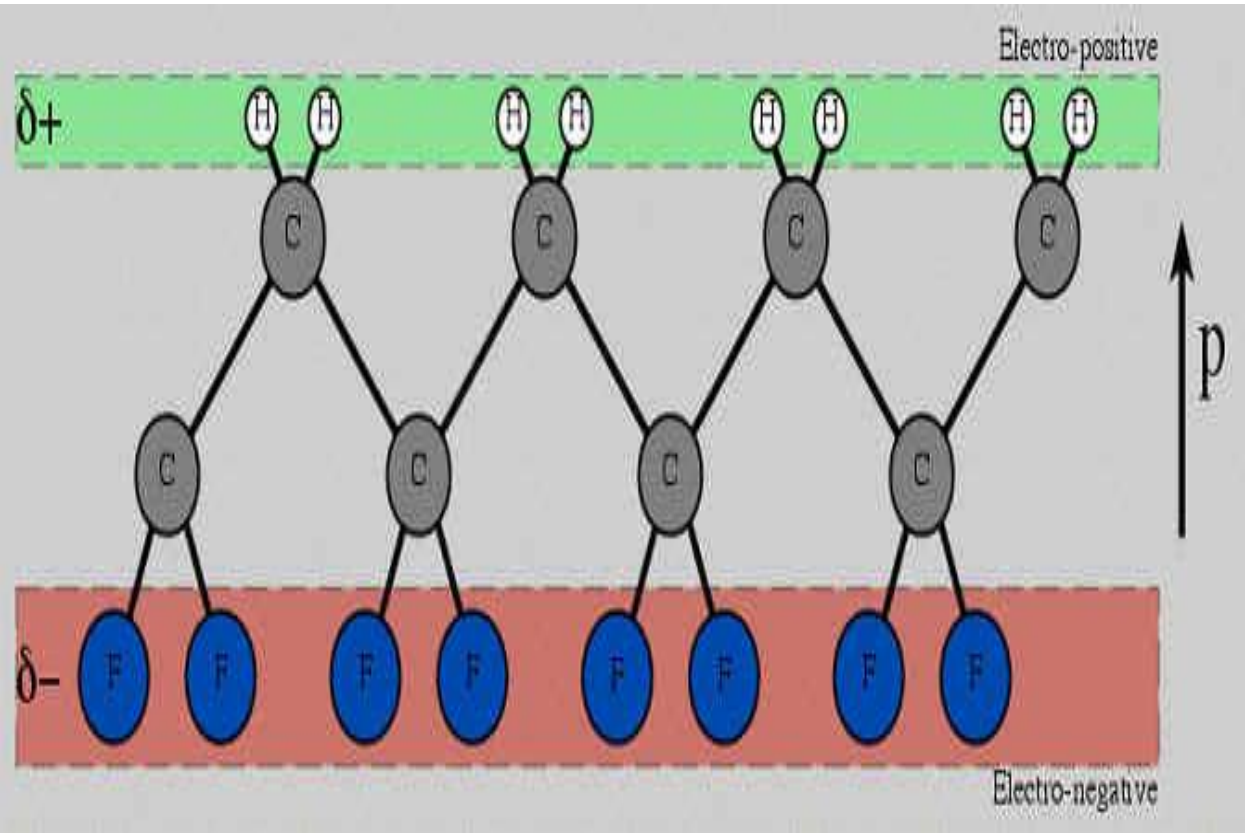


Figure 3: Alignment of molecules when external force is applied

## 2.4 Graphene

Carbon is the fourth most abundant element present on earth. The diversity in bonding makes it the most important element in a variety of disciplines. Its catenation property, i.e. the ability to form stable frameworks of interconnecting bonds with varying hybridization allows it to form innumerable compounds having different dimensionalities. A recent addition in this large family of carbon allotropes is Graphene, which is a two-dimensional monolayer of $sp^2$ carbon atoms arranged in a honeycomb like lattice. It can be considered as the parental compound for carbon allotropes of other dimensionalities. Three-dimensional graphite can be obtained by stacking the layers of graphene, which is stabilized by weak interlayer interactions.

Graphene has made it possible to understand many properties in low-dimension. It has not only opened high possibilities in electronic device's fabrication but has also shown much promise to replace silicon-based electronics. A number of other fascinating properties including the breakdown of adiabatic Born–Oppenheimer approximation, observation of integer quantum Hall effect at room temperature, realization of Klein paradox, possibilities of high superconductivity, ballistic electronic propagation, metal-free magnetism, charge-carrier doping, high surface area and chemical activities, have made graphene the material of the 21$^{st}$ century. Such diverse structural and electronic features and exciting applications have attracted scientists from all over the world to explore this low dimensional material. It is the mother of all graphitic forms and has become one of the most exciting topics of research in the last 5 to 6 years. This two-dimensional material constitutes of a new nanocarbon comprising with layers of carbon atoms making six-membered rings.[39]

Graphene is very different from carbon nanotubes and fullerenes, which exhibits properties that have fascinated the scientific community. Some important properties of graphene are an ambipolar electric field effect along with ballistic conduction of charge carriers, fractional quantum Hall effect at room temperature, tunable band gap and high elasticity. Although graphene is considered to be perfectly flat, ripples occur because of thermal fluctuations.

Ideally, graphene is a single-layer material, but graphene samples having two or more layers are being investigated with equal interest. One can give three types of graphenes: single-layer (SG), bi-layer (BG) and few-layer graphene (with number of layers ≤ 10). Although SG and BG graphene were first obtained by micromechanical cleavage, since then, graphenes containing varying number of layers have been prepared using diverse strategies.

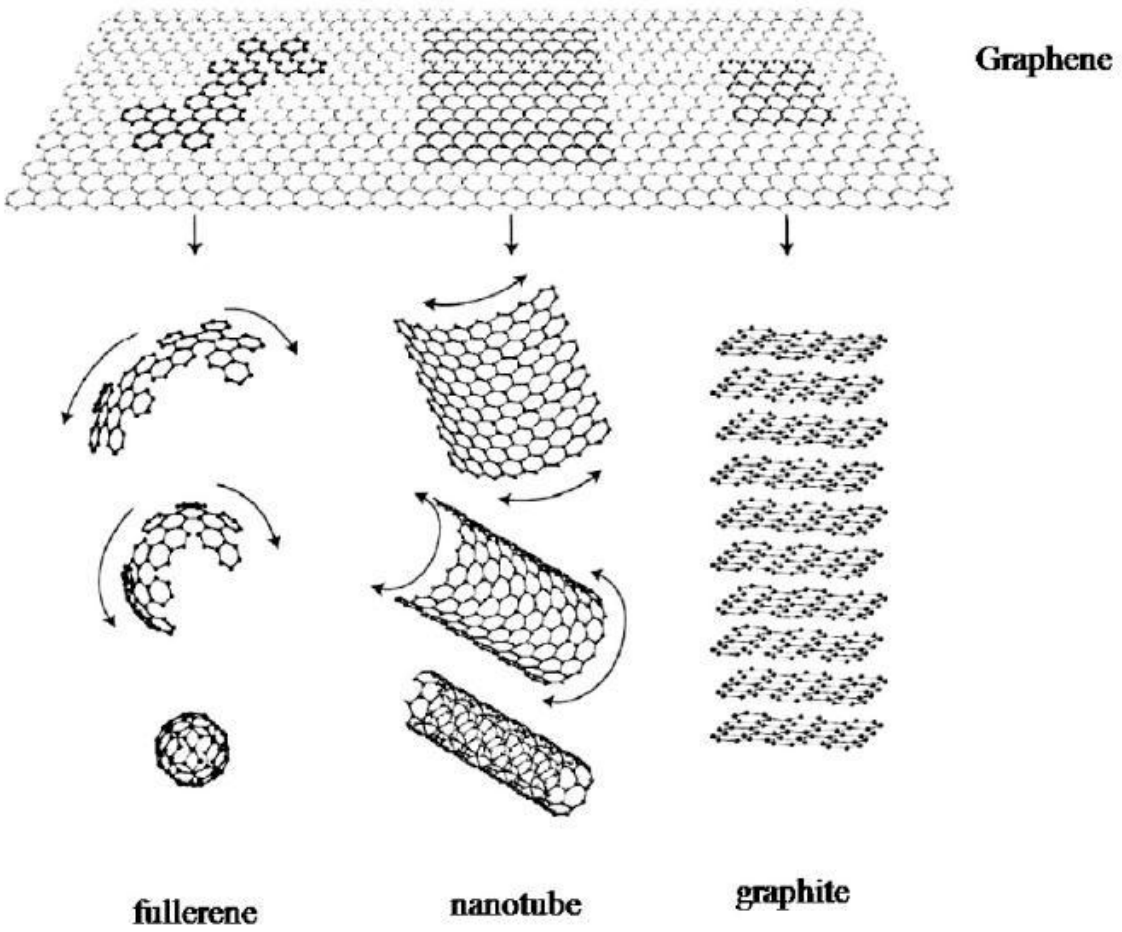


Figure 4: Graphene: mother of all graphitic forms

## 2.5 Various Methods for Synthesis of Graphene

There are a number of methods available for the synthesis of graphene. The size and quality of the produced graphene depends on the techniques used and below are some of the commonly used methods.

1. Chemical Vapor Deposition (CVD) approach

CVD approach has been by far the most effective technique to produce large scale, high quality, graphene that can be integrated into the Si device flows.

The CVD based synthesis of graphene typically involves a thin layer of a transition metal (usually few hundred nanometers thick) to be deposited on a substrate e.g. $SiO_2$. The substrate is then put in a furnace to heat it up to 1000º C in a hydrocarbon gas environment. The transition metallic layer here catalyzes the decomposition of hydrocarbon gas and then the dissociated carbon atoms gradually get absorbed into the metal layer or get diffused/remain on the metal surface depending on the metal. Many different transition metal catalysts, (e.g. Ru, Ir, Ni, Cu, Pd) have been used to synthesize graphene and the following two distinct growth mechanisms have been used . [40]

**1.** Precipitated growth is a mechanism in which the decomposed Carbon atoms dissolve in the catalyst first and then get precipitated onto the metal surface to form graphene, during subsequent cooling. This happens because the solubility of carbon in the metal decreases with decreasing temperature and the concentration of carbon decrease exponentially from the surface to the bulk. The follow-up cooling helps the carbon atoms to get segregated onto the metal surface to form graphene.

**(II)** Diffusive mechanism is a mechanism in which the decomposed Carbon atoms remain or diffuse on the metal surface and then get incorporated into graphene directly.

2. Exfoliation method

This is one of the earliest and simplest methods consisted in micromechanical exfoliation of graphite. Layers of graphene are peeled off using a Scotch tape from highly ordered graphite and then deposited on a substrate e.g. $SiO_2$. This is a very simple yet efficient method, as graphene is obtained from the highly ordered graphite crystals. Graphene extracted by this method shows very good electrical and structural quality. However, the shortcoming of this method is its non-scalability and unevenness of graphene films with a small area.

3. Epitaxial growth

Graphene is synthesized by annealing of SiC crystal at a very elevated temperature (at ~2000 K) in an ultra-high vacuum. The thermal desorption of silicon from the top layers of SiC crystalline wafer yields a multilayered graphene. The number of layers of graphene can be controlled by limiting the time or the temperature of heating treatment. The quality and the number of layers in the sample depends on the SiC face used for its growth. Although the produced structure has a larger area than the one obtainable by the exfoliation technique, but still the area is way below the size that is required in electronic applications. Moreover, it is difficult to functionalize graphene that is obtained by this method.

4. Wet-chemistry approach

The Wet-chemistry based approach is also used to synthesize graphene by the reduction of chemically synthesized graphene. The graphite is transformed to acid-intercalated graphite oxide via severe oxidative treatment in nitric and sulphuric acid. The intercalant formed is then rapidly evaporated at elevated temperatures, which is followed by its exposure to ball milling or ultrasound. Exfoliation of the graphite oxide readily occurs in an aqueous medium due to the hydrophilicity of the former. The subsequent reduction of exfoliated graphite oxide sheets by hydrazine results in precipitation of graphene owing to its hydrophobicity. This method is more versatile than other methods comprising exfoliation and epitaxial growth on SiC and is easier to scale up. Still, it has a poor control on the number of layers of graphene synthesized.

## 2.6 Properties of Graphene

The distinctive thermal, mechanical and electronic properties of graphene make it a promising candidate for wide range of applications in nanotechnology and nanoscience. The versatile properties of graphene are well documented in the fast growing scientific literature. Some of its technological implications and interesting properties are:

1. Electronic properties

Graphene has high potential for electronics because of its extraordinarily high mobility of charge carriers at room temperature. Now, when Si-based technology is approaching its fundamental limits, graphene appears to be an ideal candidate to take over the charge from silicon. Still, graphene is semi-metallic with no band gap, which greatly limits its applications in the field of electronics due to its high leakage current . The electronic band gap plays an important role in modern device physics and technology and it controls the performance of semiconductor devices. Also, it is a property that is inherent to insulators and semiconductors which considerably governs their transport and optical properties. It is now been possible to open and tune-up the band gap of graphene bilayers by applying external electric field.

The most useful property of graphene is that it is a zero-overlap semimetal i.e. with both holes and electrons as charge carriers that provide very high electrical conductivity. The carbon atoms have a total of six electrons, out of which, four are there in the outer shell and two are in the inner shell. The 4 outer shell electrons in a carbon atom are available for chemical bonding, but in graphene, each carbon atom is connected to three other carbon atoms on the two-dimensional plane, leaving one electron being available in third dimension for electronic conduction. The electronic mobility of graphene is very high, with previously reported result to above 15,000 $cm^2 \cdot V^{-1} \cdot s^{-1}$ It is also said that graphene electrons act like photons in terms of mobility due to lack of mass. These charge carriers can travel even sub-micrometer distances without any scattering; a phenomenon that is known as ballistic transport. Also, the structural manipulation may bring in optical properties (i.e band-gap opening), which in turn can get incorporated into it, resulting in a potential suitable for opto-electronic applications.[41]

2. Optical properties

Graphene can absorb 2.3% of white light, is a unique and interesting property, considering that it is only 1 atom thick. This property is due to it's before mentioned electronic properties; the electrons act like massless charge carriers with high mobility. Few years ago, it has been proved that the amount of white light absorbed by graphene is based on the Fine Structure Constant. Adding more layers of graphene increases the amount of white light absorbed by graphene, which is approximately the same value (2.3%) as before.

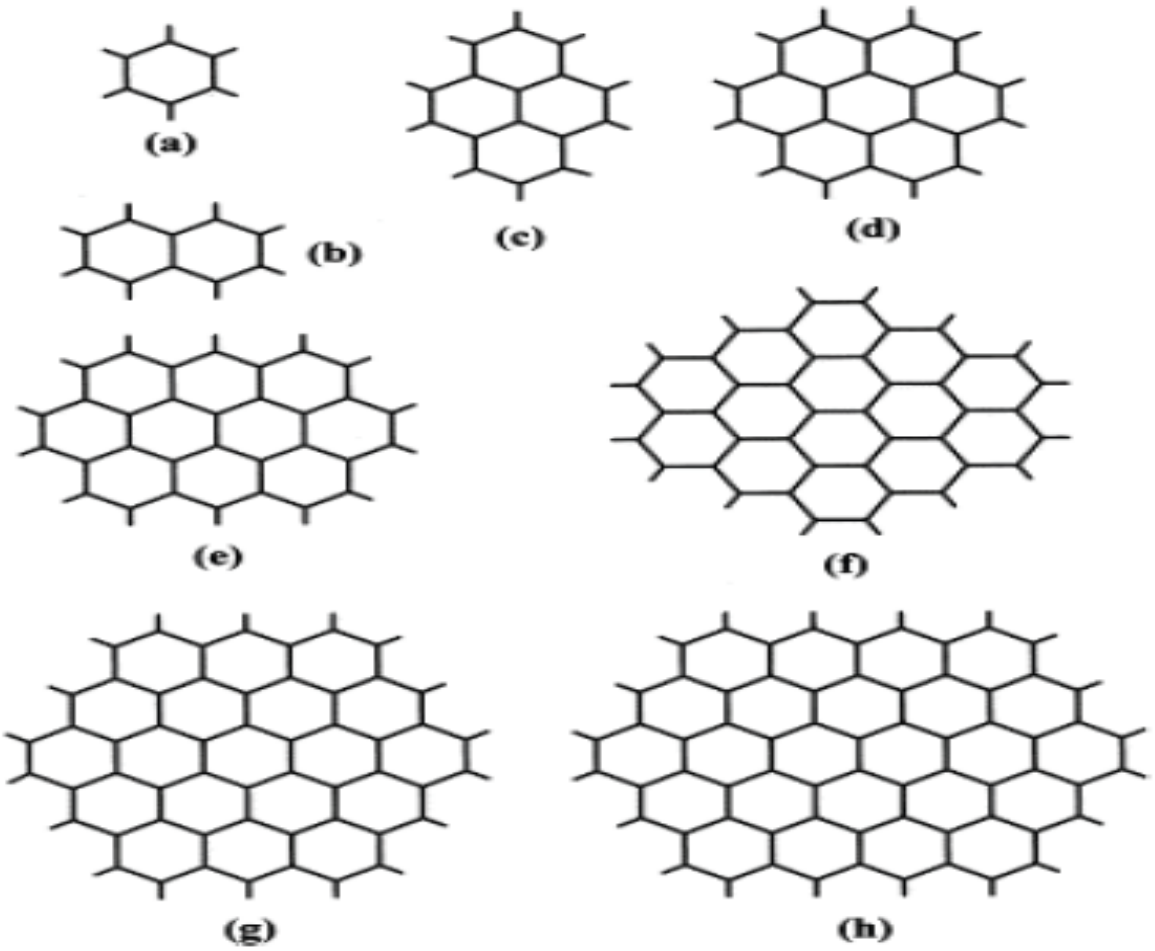


Figure 5: Models for hexagonal clusters: (a) $C_6H_6$, (b) $C_{10}H_8$, (c) $C_{16}H_{10}$, (d) $C_{24}H_{12}$, (e) $C_{32}H_{14}$, (f) $C_{42}H_{16}$, (g) $C_{54}H_{18}$ and (h) $C_{66}H_{18}$.

3. Mechanical Properties

Graphene has received the title of "strongest material ever" after the confirmation of its breaking strengths of 42 N/m with mechanical strain of up to ~ 25% and Young's modulus of Y ~ 1.0 TPa. Its mechanical properties can also be controlled as demonstrated by stress measurements performed on graphene sheets that were subjected to deformations induced by depositing different insulating layers. The research related to the mechanical features of graphene has been confirmed by several works using different techniques. Among them are molecular dynamics, tight binding, simulations, and semiempirical models, these have estimated the Young's modulus and other intrinsic mechanical properties of graphene. [42]

These outstanding mechanical properties of graphene have attracted great interest in electronic applications due to the potential that these light and flexible materials offer for designing building components in nano-electromechanical systems (NEMS). The fabrication of cheap NEMS devices requires a complete correspondence between electrical and mechanical responses of the conductive channel. In this way, the operational mechanism of an efficient NEMS based on graphene depends on feasibility of performing band gap engineering with an aid of external mechanical forces.

Another one of graphene's stand-out properties is its strength. Because of the strength of its 0.142 Nm-long carbon bonds, it is the strongest material discovered, with a tensile strength of 130,000,000,000 pascals, as compared to 400,000,000 pascals for A36 structural steel, or 375,700,000 pascals for Aramid (Kevlar). Not only graphene is extraordinarily strong, also it is very light. It is also said that a single sheet of graphene , which is sufficient in size to cover a whole football field, would weigh under 1 gram.[43]

4. Magnetic Properties

There is a considerable interest on the magnetism of nanographite particles. Enoki *et al.*. stated that edge states as well as of adsorbed species play an important role in determining magnetic properties of nanographite particles. Recently, the magnetic properties of the samples prepared by the method exfoliation of graphite oxide, conversion of arc evaporation of graphite, nano-diamond and partial chemical reduction of graphene oxide have been studied. The Magnetic properties of graphene reveal that the dominant ferromagnetic interactions coexist with antiferromagnetic interactions in all the samples, somewhat like in phase-separated systems.

Graphene is not known for its magnetic properties beause of its many other useful properties but over the past few years researchers have shown considerable amount of interest in utilizing the magnetic properties of graphene. By optimizing all its electrical, mechanical, optical, and magnetic properties, graphene can be used in vast amonut of applications that no other material has been used especially in the field of nanoscience and nanotechnology.[44]

## 2.7 Application of RGO/PVDF/Fe Composite film

PVDF transducers have an advantage of being more suitable for modal testing applications as compared to semi-conductor piezoresistive transducers, and more compliant for structural modification than piezoceramic transducers. For these reasons, the use of RGOPVDF/Fe composite as active sensors is a keystone for the development of future structural health monitoring methods, security methods, energy harvesting method, etc., due to their low cost and compliance.[2]


Figure 6: Applications of RGO/PVDF/Fe composite

## 2.8 Circuit diagram

The circuit diagrams that can be used for amplification of the generated voltage are given below.

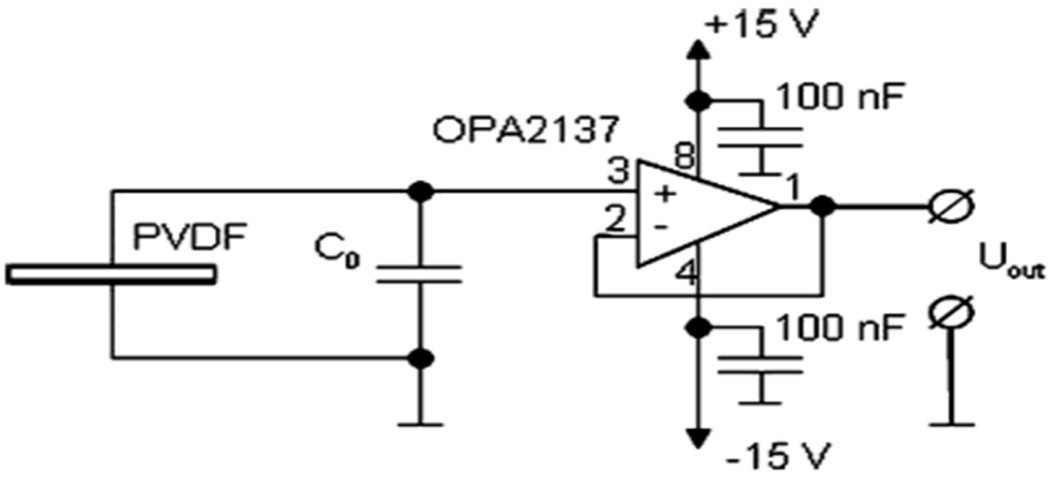


Figure 7: Circuit diagram of charge amplifier

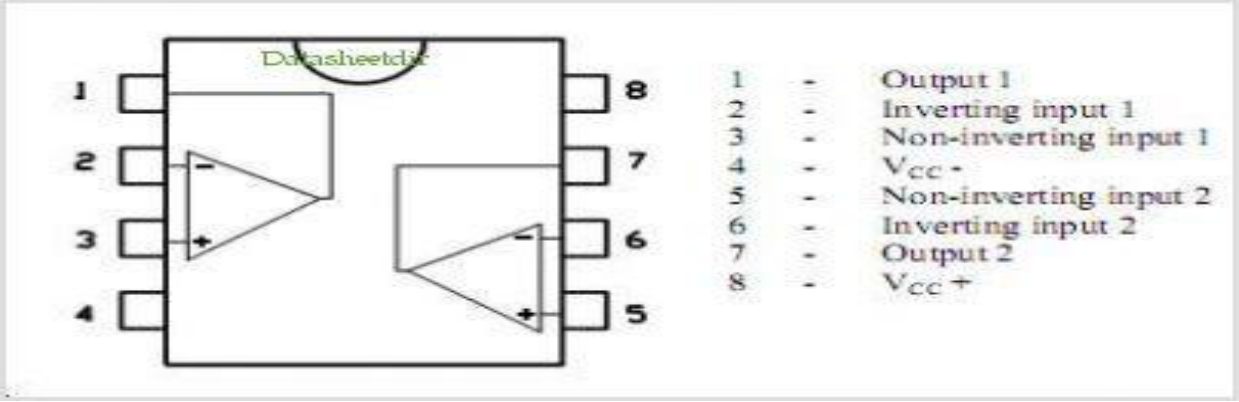


Figure 8: Pin diagram of OPA2137.

The output voltage i.e. $U_{out}$ can be calculated from the following equation:

$U_{out}=Q/C_o$

Where, Q is the charge generated by the composite film

$C_o$ is the capacitance in the corresponding electronic circuit

$U_{out}$ is the voltage obtained at the output

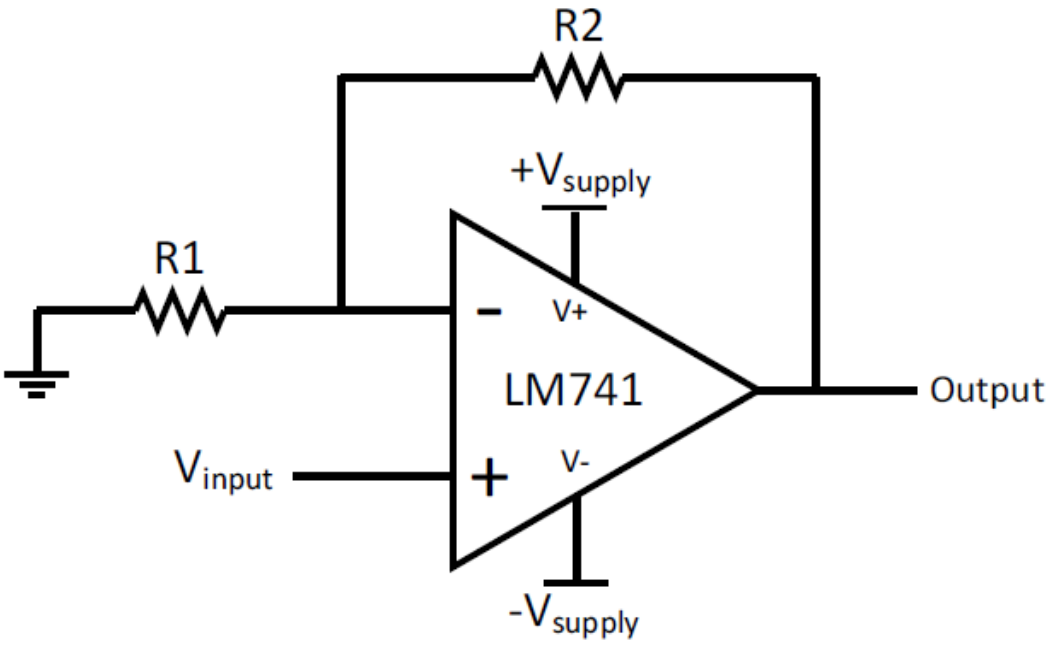


Figure 9: Circuit diagram of voltage amplifier

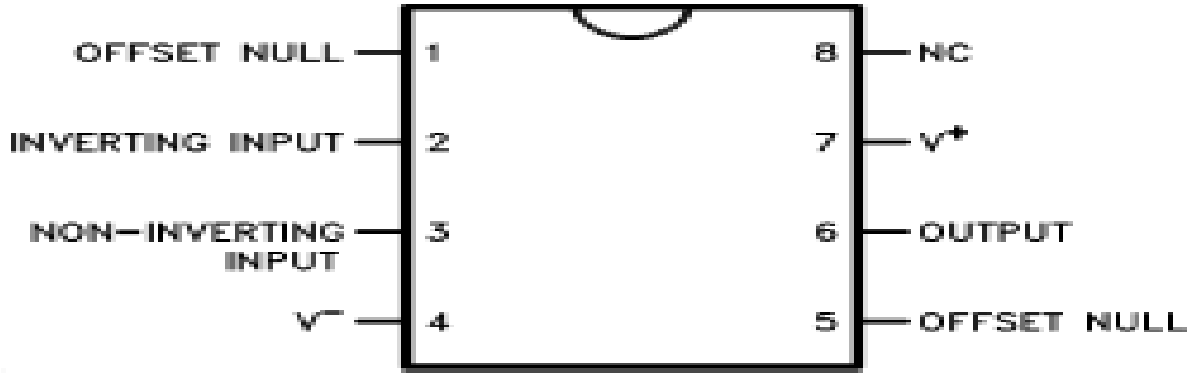


Figure 10: Pin diagram of IC 741

Gain $=(1+R_2/R_1)$

Where, R1=input resistance

R2=feedback resistance

Both the circuit diagrams were used but the circuit with LM741 is low cost and easy to make.

# *CHAPTER 3*

# Methodology

This chapter describes the various materials and methods used for the synthesis of GO then RGO from GO and then the preparation of RGO/PVDF/Fe composite film.

## 3.1 Materials:

### 3.1.1 Preparation of Graphene Oxide (GO)

Graphite flakes (Asbury Carbons), Sulfuric acid (98%, ACS), Hydrogen peroxide (40% wt, Emplura), Potassium permanganate (99%, Merck Specialties Pvt. Ltd.), Hydrochloric acid (35%, Sigma Aldrich Pvt. Ltd.), Distilled water.

### 3.1.2 Preparation of Fe doped RGO from GO

Graphite flakes (Asbury Carbons), Hydrochloric acid (35%, Sigma Aldrich Pvt. Ltd. ), Fe (300 mesh CDH).

### 3.1.3 Preparation of Fe doped RGO/PVDF Composite film

Graphite flakes (Asbury Carbons), potassium permanganate ($KMnO_4$, (99%, Merck Specialties Pvt. Ltd. ), sodium nitrate ($NaNO_3$) and Fe powder (Loba Chemie, India). Graphine oxide (GO) and Fe-doped reduced graphine oxide (Fe-RGO) (laboratory synthesized, the detail procedure and relevant characterization is provided in experiment section of the ESI). (PVDF) (Alfa-Aesar, India). sulphuric acid ($H_2SO_4$) , N, N dimethyl formamide (DMF), ethanol ($C_2H_5OH$) and hydrogen peroxide ($H_2O_2$) (Merck Chemicals, India).

## 3.2 Methods

### 3.2.1 Synthesis of Graphene Oxide

1. Conc. sulfuric acid (46 mL) is added to a round-bottom flask of 250 mL at 0−5 °C.

2. Then, 2 g of natural graphite flakes is added and then stirred at this temperature to form a homogeneous suspension.

3. About 6 g of potassium permanganate is added very slowly over a time span of 20−25 min followed by stirring for 2 hour.

4. The temperature of the reaction system is maintained at 0−5 °C with an ice bath.

5. The flask is then transferred to a preheated oil bath at 35°C with constant stirring for 12 h.

6. About 92mL of distilled water is added very carefully followed by additional stirring for 1 h.

7. The deep brown reaction mixture is added to 240 mL of distilled water followed by addition of 30% hydrogen peroxide until the color is changed to bright yellow.

8. Finally, a 5% hydrochloric acid solution is added to remove the manganese ions from graphite oxide followed by washing with distilled water to remove excess acid.

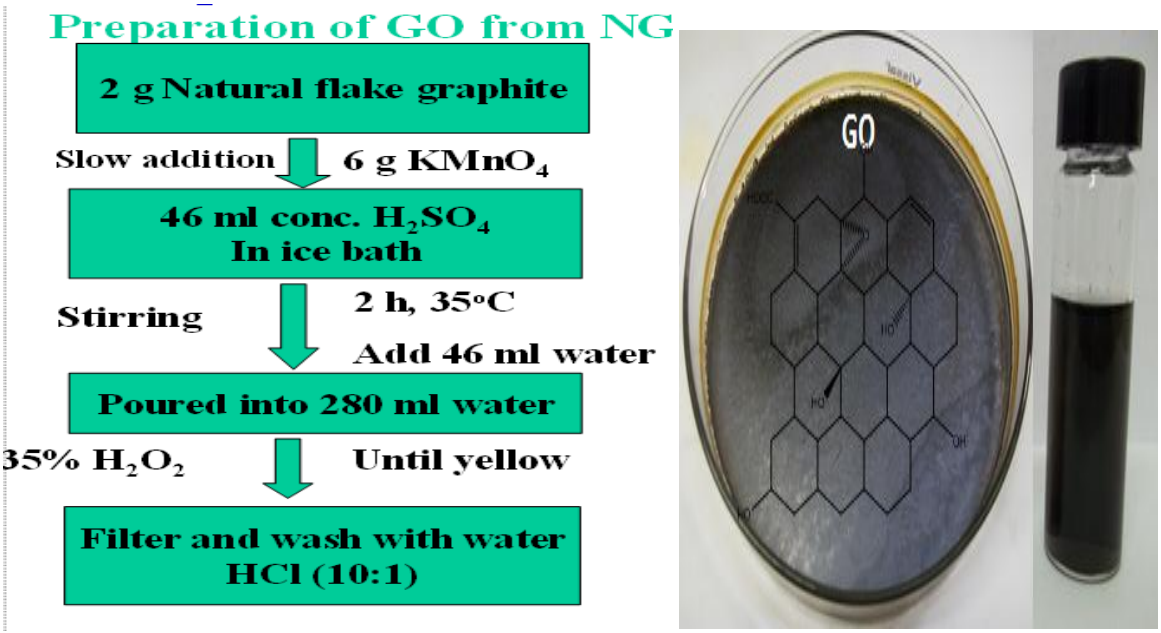


Figure 11: (a) Flow diagram for GO synthesis, (b) Diagram showing GO film in petri dish.

### 3.2.2 Synthesis of Fe doped RGO

1. RGO is synthesized by the reduction of GO in the presence of iron powder and HCl.
2. At first, as prepared GO (0.5 mg/ml) is dispersed in distilled water through ultrasonication.
3. Then, water dispersed Fe powder (5 g) is added to the suspended GO and continued ultrasonication for 90 m.
4. After that, 100 ml of HCl solution (35%) is added in the GO mixture and sonicated for another 90 min.
5. The resulting solution is filtered and washed with distilled water (to maintain pH ≈ 7) and ethanol for several times.
6. Finally, the obtained solid is dried in vacuum oven at 60 ºC for 24 h.
7. During the reduction process, some Fe particles were incorporated into the surface of RGOs, as confirmed by XRD analysis.
8. We assume that Fe not only reduced the GO to RGO, but also remain present in RGO as a dopant. RGO containing mixture of Fe and Fe-oxide is referred as Fe doped RGO.
9. Similarly with different Fe loading (0.0g, 0.1g, 0.5g and 1.0 g) Fe doped RGO is prepared to vary the conductivity of the composite.

### 3.2.3 Synthesis of Fe doped RGO/PVDF composite film

1. Fe-RGO is dispersed in DMF (1 mg/ml) using ultrasonicator for 5 h.
2. Separately, PVDF (0.3g) is dissolved in DMF at 90 ºC.
3. The PVDF solution is then mixed with the Fe-RGO solution (mass ratio of Fe-RGO and PVDF is 1: 3).
4. The resulting solution is kept under ultrasonication for 5 h.
5. Afterwards, the well disperse solution is poured onto petri dish and kept in vacuum oven at 120 ºC for 20 h for complete removal of solvent.
6. Finally, dried Fe-RGO/PVDF composite film is obtained.
7. Likewise, different Fe loading (0.0g, 0.1g, 0.5g and 1.0 g) are prepared and abbreviated as $PVDF/RGO_{0.1}/Fe_{0.0g}$, $PVDF/RGO_{0.1}/Fe_{0.1g}$, $PVDF/RGO_{0.1}/Fe_{0.5g}$, $PVDF/RGO_{0.1}/Fe_{1g.}$
8. Similarly the amount of RGO is varied (0.0g, 0.05g, 0.1g, 0,3g) keeping Fe constant and an optimum amount of energy was generated.

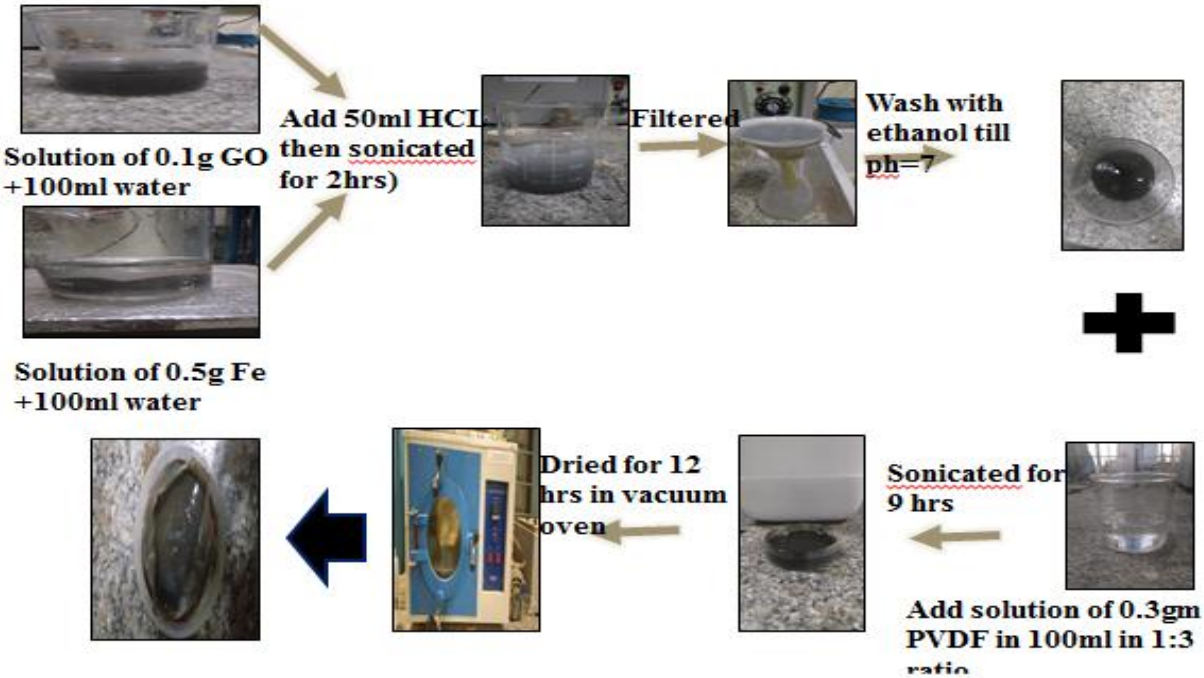


Figure 12: Flow diagram for synthesis of RGO/PVDF/Fe composite film.

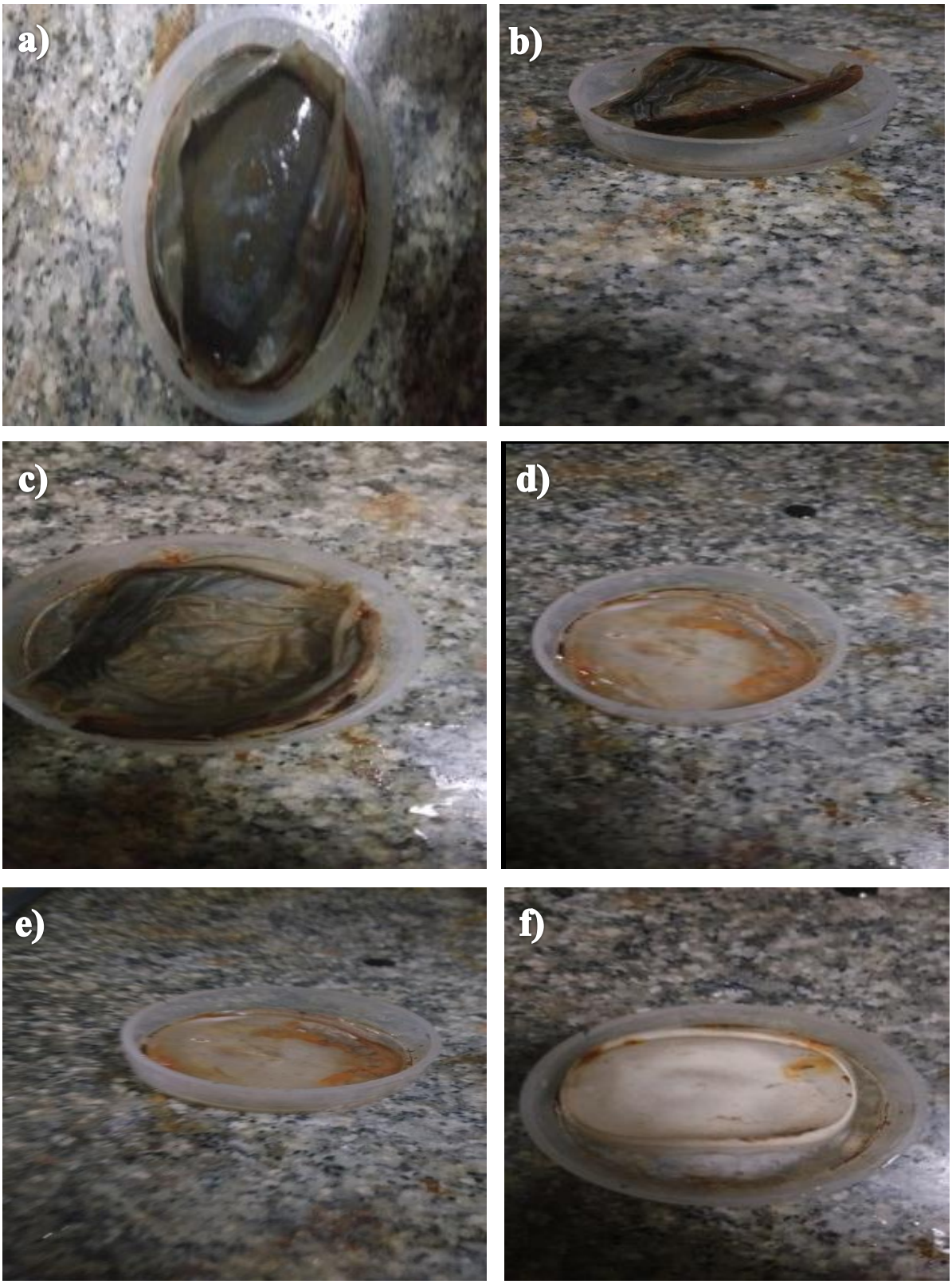


Figure 13: (a) RGO/PVDF/$Fe_{0.1g}$ film, (b) RGO/PVDF/$Fe_{0.5g,}$ (c) RGO/PVDF/$Fe_{1g}$ (d) PVDF/$Fe_{0.5g}$, (e) PVDF/$Fe_{1g}$ (f) PVDF/$Fe_{2g}$

### 3.2.4 Synthesis of Fe doped PVDF composite film using water

1. PVDF (2 g) is dissolved in DMF at 90 ºC.
2. Fe powder if different weight (0.0g, 0.1g, 0.3g, 0.5g, 1.0g and 2.0g) was added to the solution and ultrasonicated for 4h.
3. The solution is poured into a petri dish and distilled water is added. The addition of water leads to immediate coagulation and a film is formed.

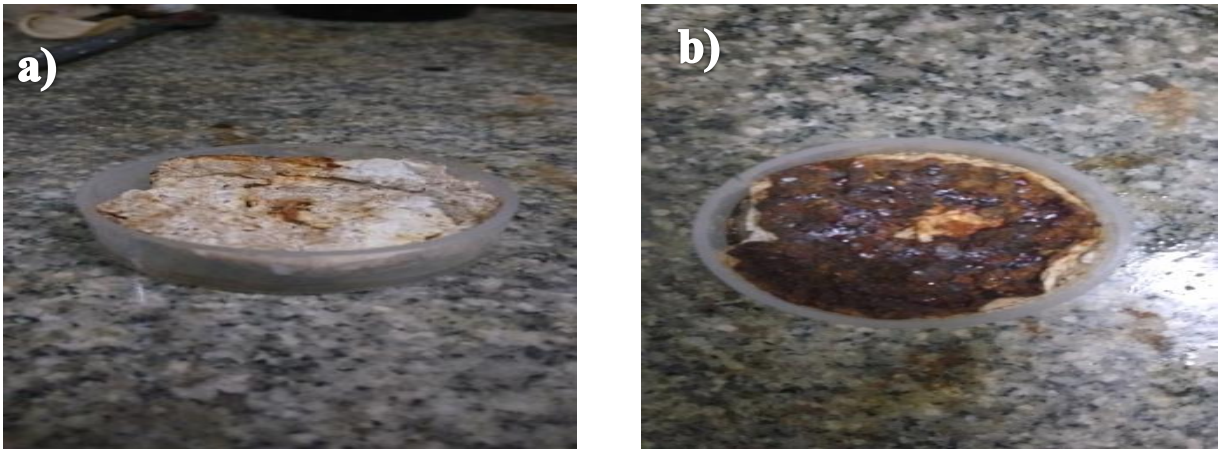


Figure 14: (a) PVDF/$Fe_{0.1g}$, (b) PVDF/$Fe_{1g}$

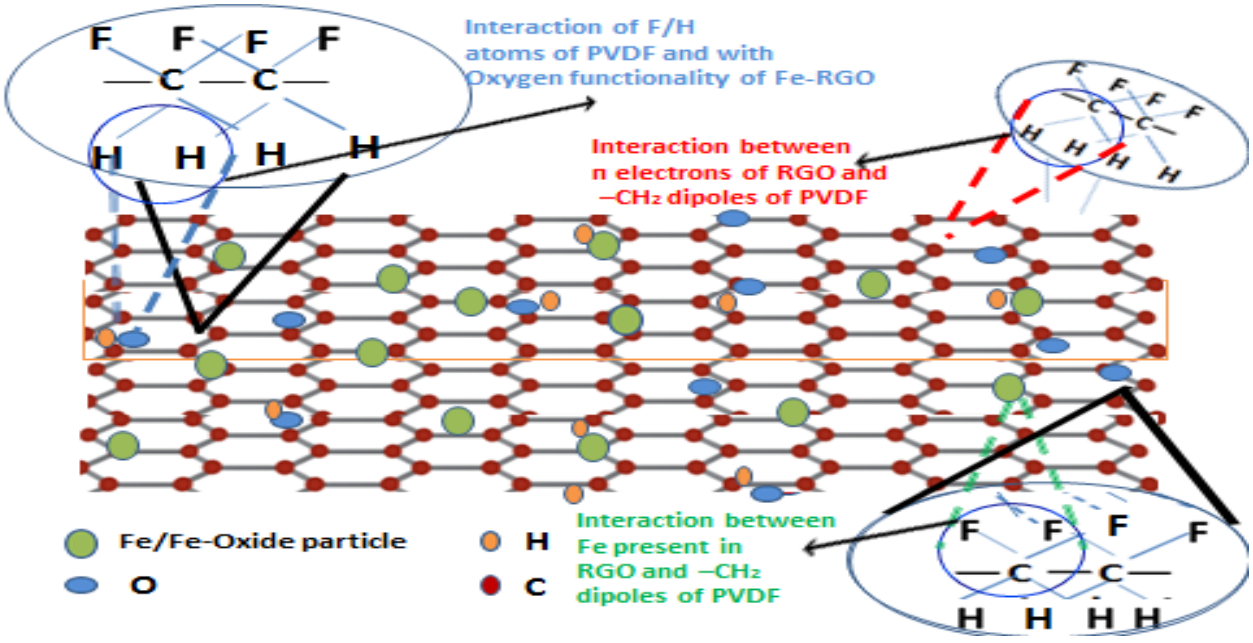


Figure 15: Representation of molecules in composite film

# *CHAPTER 4*

# Characterization techniques:

## 4.1 X-ray Diffraction (XRD) analysis:

X-ray powder diffraction (XRD) analysis is utilized to determine polymorphism in crystalline organic materials. Its stability is an important issue in the manufacturing and performance of the imaging materials and devices. A common problem that still exists in organic materials is polymorphism, which is the ability of a singular molecular species to get crystallized in more than one crystal structure. These multiple structures are the result of different packing configurations of molecule in a crystal. The pseudo-polymorphism is variation of polymorphism, where a solvent molecule is a part of the lattice that results in crystal structure change.

To understand the presence or absence of polymorphism in the organics, X-ray diffraction (XRD) is used as a method of choice to identify these crystal phase modifications. It should be understood that if a material is amorphous, the XRD then may provide minimal information related to polymorphism. X-ray diffraction is a powerful method to study nano-materials. The wavelength of the X-rays is on the atomic scale, therefore X-ray diffraction (XRD) is just a primary tool for probing structure of nano-materials.

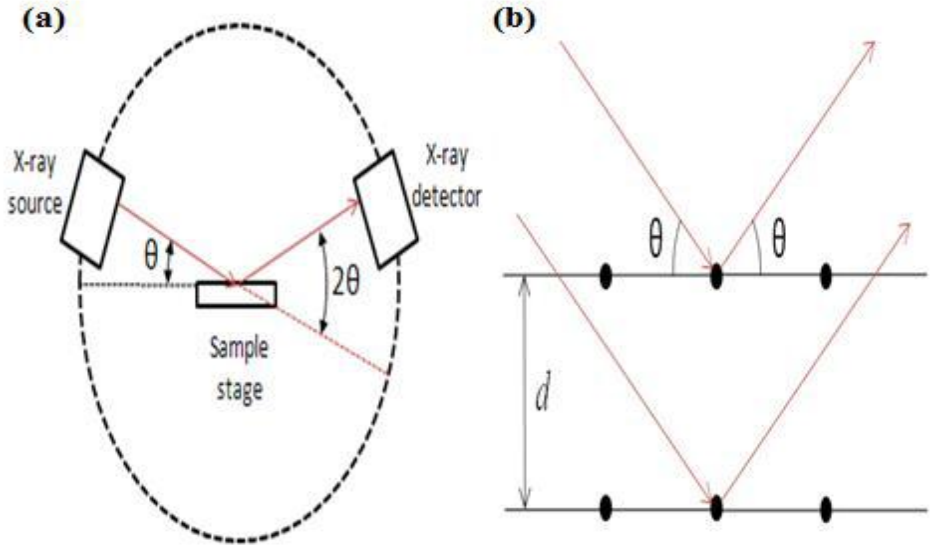


Figure 16: Basic features of (a) X-ray diffractometer , (b) Bragg‘s law.

The lattice planes in the simple crystal are separated by a distance d. Bragg‘s law relates the wavelength (λ) of the reflected X-rays, spacing between their atomic planes (d) and the angle of diffraction (ɵ) as:

$2d \sin ɵ = n \lambda$

The angle between the two beams i.e. the transmitted beam and diffracted beam will always be equal to 2ɵ. This angle is obtainable in experimental situations and hence the results of X-ray diffraction are given in terms of 2ɵ. It is however important to remember that the angle used in the Bragg‘s equation should correspond to the angle which is between the incident radiation and the diffracting plane, that is called ɵ.

For first order diffraction, n=1, and knowing ɵ and λ, we can calculate the interplanar spacing d–value for a plane. The first step of X-ray diffraction pattern is the indexing of XRD peaks. Indexing is assigning the correct Miller indices to every peak of the diffraction pattern. There are three methods for indexing a diffraction pattern; these are (i) comparing the obtained XRD pattern with the standard data base (JCPDS-cards) (ii) analytical method (iii) graphical method. The intensity of the diffraction signal is plotted against the diffraction angle 2 ɵ.

XRD studies for this project have been carried out using Bruker D8 Advance Diffractometer with Ni-filtered Cu Kα radiation (DTU, Delhi) with Voltage- 30 kV, 35 mA.

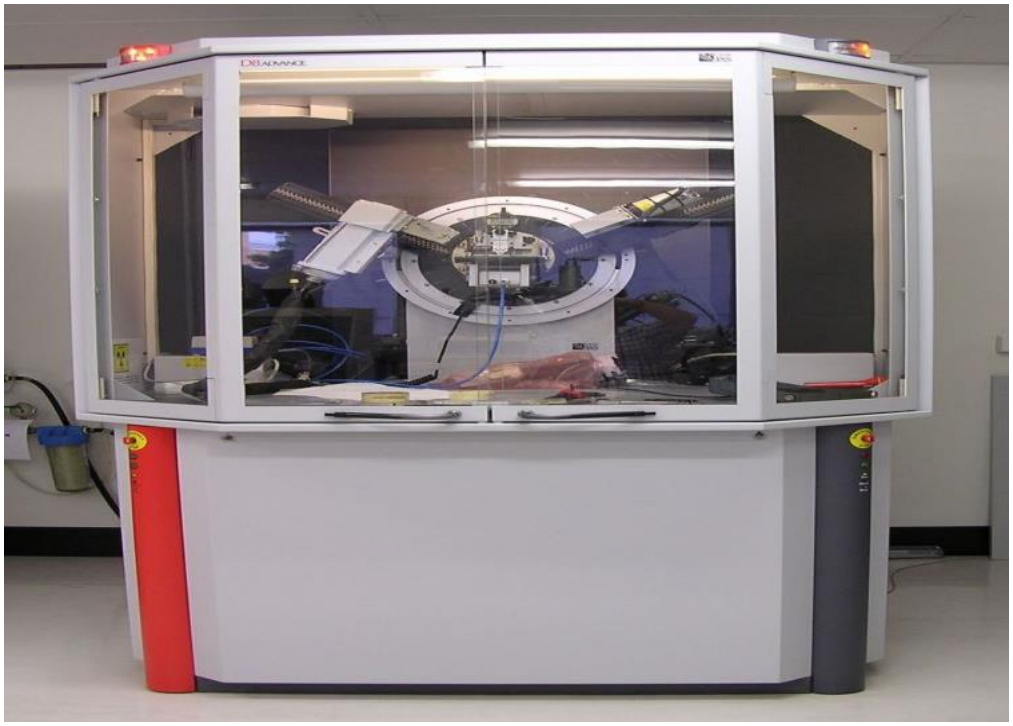

Figure 17: X-ray diffraction machine in DTU.

**4.2 Fourier transform infrared (FT-IR) spectroscopy:**

FTIR spectroscopy is a very powerful technique to study the molecular orientation and ordering. The Infrared (IR) spectroscopy detects vibration characteristics of the chemical functional group in a sample. When infrared radiations are passed through a sample, some of the radiations are absorbed by the sample and some of are passed through or transmitted. The resulting spectrum thus represents molecular absorption and transmission, thus creating a molecular fingerprint of the sample.

There are only two kind of fundamental vibrations for the molecules: stretching, i.e. the distance between two atoms either increases or decreases, but atoms remain in the same bond axis, and bending, in this the position of the atom changes with respect to the original bond axis. The stretching and bending vibrations of a bond occur at certain frequencies. When the infrared light of that same frequency is incident on the molecule then energy is absorbed and thus the amplitude of that vibration gets increased. When the molecule goes back from the excited state to the original ground state then that absorbed energy is released as heat. So after interaction of infrared light with the material, the chemical bonds will stretch, contract and bend. As a result, a particular chemical functional group tends to adsorb infrared in a specific wavenumber range despite of the structure of the rest of the molecule. For example, the C=O bond stretch of a carbonyl group appears at 1700cm-1 in a various molecules. Hence, this correlation of bond and the wavenumber position with the chemical structure is used to find functional group in sample.

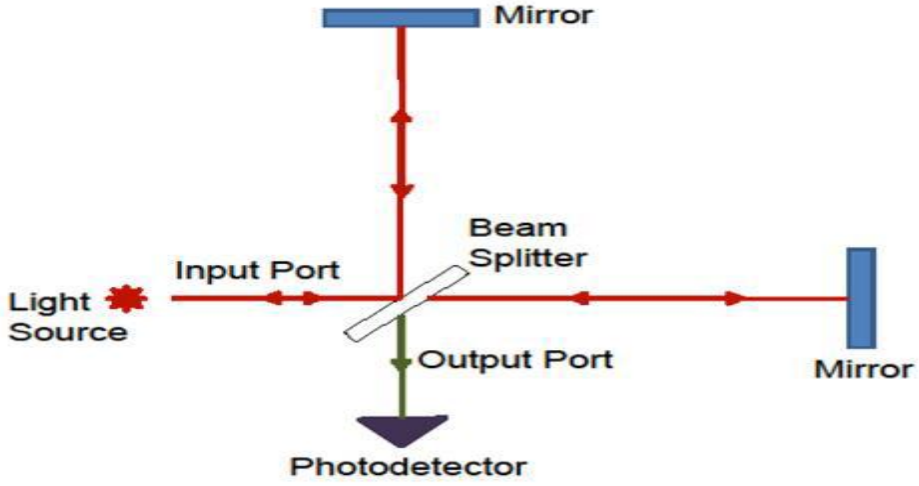


Figure 18: Representing principle of FTIR spectroscopy

A beam splitter is used to divide the laser light entering from the input port into a transmitted beam and then to a reflected beam, perpendicular to each other. At the end of both beam's path, there is a mirror that reflects the light towards the beam splitter. If both the beams paths have exactly the same length, then the beams electric fields oscillate in same phase when the light returns to beam splitter. The beams then recombine to produce a beam which exits the beam splitter from the output port but if the two paths differ in length even by half a wavelength, then they are out of phase so in this case, they interfere destructively at the beam splitter hence no light exits from output port.

FTIR studies for this project have been carried out using Thermoscientific Nicolet 380(DTU, Delhi).


Figure 19: Thermoscientific Nicolet 380 at DTU, Delhi.

### 4.3 Scanning Electron Microscopy (SEM):

A scanning electron microscope machine operates at a high vacuum. Its basic working principle is that a beam of electrons is generated by a source, typically a tungsten filament or via field emission gun. This electron beam is accelerated through a high voltage and is passed through a system of many apertures and electromagnetic lenses to produce a single thin beam of electrons. Then this beam scans the surface of the specimen by means of scanning coils

Electrons that get emitted from the specimen by the action of the scanning beam are collected by a suitably-positioned detector. Meanwhile, the microscope operator is watching the image on a screen. The key to the working of scanning electron microscope is that the beam scanning the specimen surface is perfectly synchronized with the spot that the operator is watching in the screen. Electron detector controls the brightness of the spot generated on the screen that the detector sees. All SEM images are black-and-white in color, though they may have false colors applied to them for some reasons or to aid interpretation.

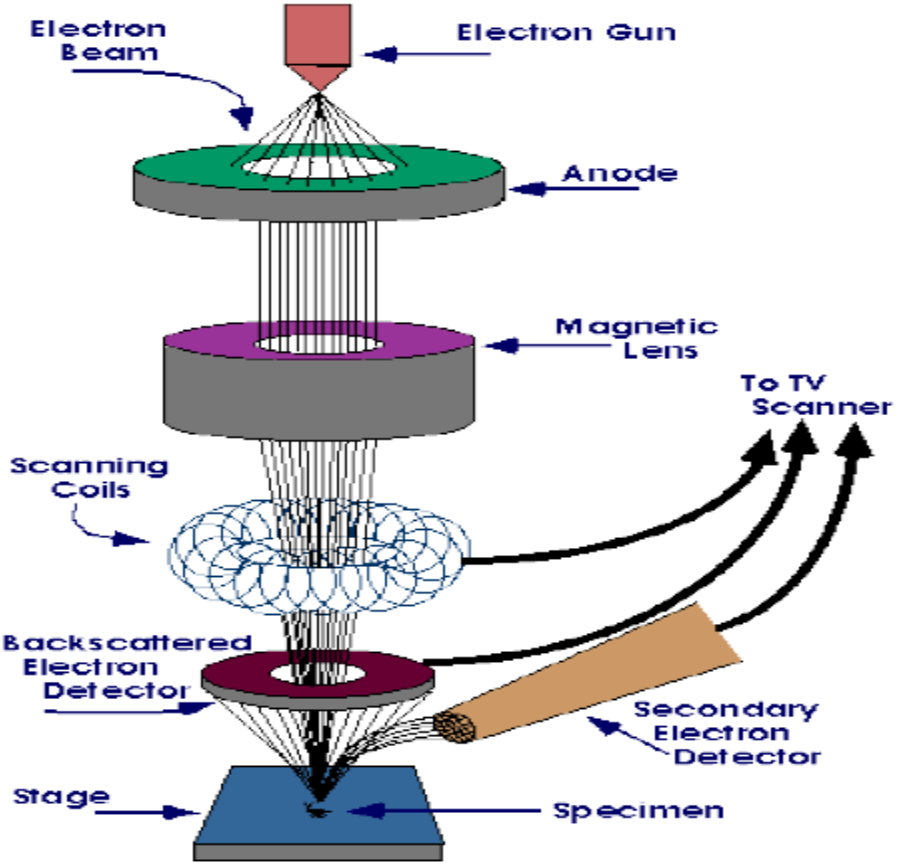


Figure 20: Schematic representation of Scanning electron microscopy

**4.4 Energy-dispersive X-ray microanalysis:**

This machine helps the operator in determining the composition of the features in the SEM image. The working principle of EDX is that an electron beam generates X-rays in the specimen. Most of these X-rays have energies characteristic similar to the elements that emitted them. Therefore, if one can measure the energy of the X-rays, the person may know which elements are present in that specimen. If we control the instrument conditions carefully we can determine not only which elements are present but also their concentrations.

There are mainly three principal components of an EDX system: the X-ray detector; the pulse processor, which measures the voltage pulses generated corresponding to the X-ray energies, and a PC. The X-ray detector is positioned so as to intercept the X-rays that are emitted from the sample. After entering the detector, X-rays generate a small current, which is afterwards converted into a voltage pulse. Now, the size of the voltage pulse generated is proportional to the energy of the X-rays. The PC measures the voltage pulses over a period of time, and plots them as a histogram. The histogram then shows a spectrum of the X-ray energies that were measured, and then by examining the spectrum, the elements present can be determined. The SEM and EDX studies for this project have been done using HITACHI, model no.S- 3700N with EDS-X with X-ray (DTU, Delhi).


Figure 21: SEM HITACHI, model no.S-3700N with EDS-X with X-ray at DTU, Delhi

**4.5 Transmission electron microscopy:**

Transmission electron microscopy is an important characterization tool for imaging nanomaterials to obtain precise quantitative measures of particle size, morphology and their distribution. TEM images are formed by the transmission of a highly focused beam of electrons through the sample. However, since electrons are used in place of light to illuminate the sample, TEM images have significantly higher resolution than light -based imaging techniques.
The amplitude and phase variations in transmitted beam provide an imaging contrast which is a function of the sample thickness and the sample material. Successful imaging of nanomaterials depends mainly on the contrast of the sample with respect to the background. The samples are prepared by drying nanomaterials on a copper grid which is coated with a very thin layer of carbon. Those materials whose electron densities that are higher than amorphous carbon are easily imaged. These materials mostly include metals (e.g., copper, silver, gold), oxides (e.g., aluminum oxide, titanium Oxide, silica) and other materials such as polymer nanoparticles, carbon nanotubes, and magnetic nanoparticles.

Transmission electron microscope (TEM) generates image by accelerating a beam of electrons which passes through the specimen. In the machine, the electrons are accelerated to 100 keV or even higher, they are projected onto a thin specimen by means of the condenser lens system, and then penetrate the sample thickness either undeflected or deflected. The biggest advantage that TEM offers is the high magnification and the ability to provide both image and information about diffraction from a single sample.

The scattering process that is experienced by electrons while passing through the specimen determines the kind of information obtained. The elastic scattering involves zero energy loss and gives rise to diffraction patterns. The inelastic interaction between primary and sample electrons at heterogeneities such as boundaries, defects, density variations, etc., causes complex absorption and scattering effects that leads to a spatial variation in intensity of transmitted electrons.
TEM studies have been done for this project with the help of FEI Tecnai S Twin.

Figure 22: TEM machine at JNU, New Delhi

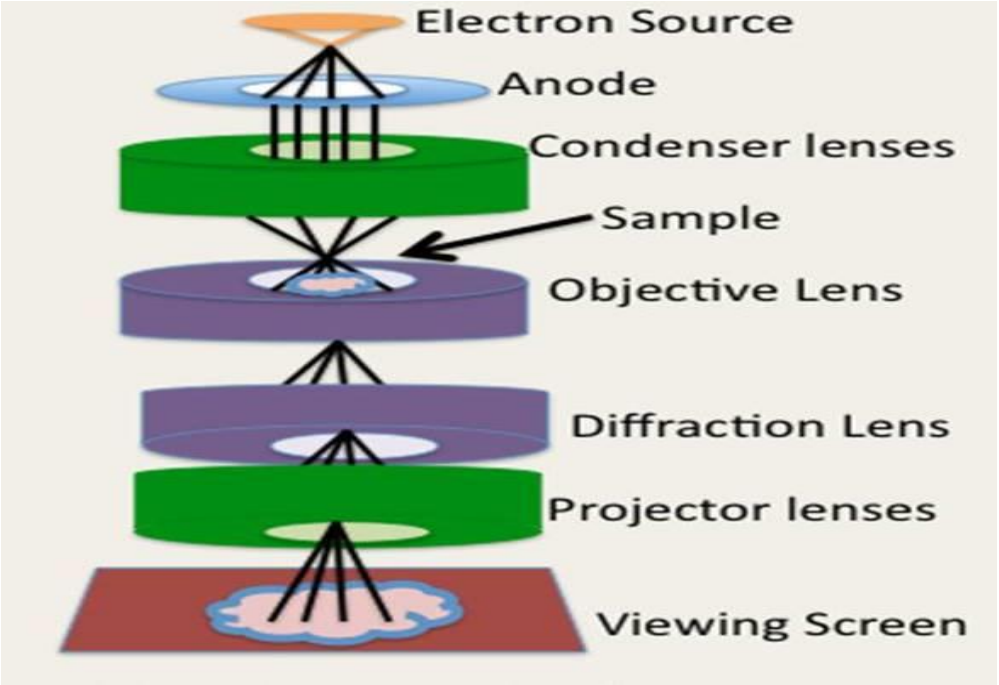


Figure 23: Main components of a TEM

# *CHAPTER 5*

# Result and Discussion

## 5.1 XRD Analysis

The X-ray diffraction (XRD) is the most widely used technique for general crystalline material characterization. It is used to Measure the average spacing's between layers or rows of atoms, determine the orientation of a single crystal or grain. The XRD pattern obtained for as synthesized GO by Hummer's method The XRD of GO clearly show a peak the diffraction peak at $2\theta=10^{0}$, which is mainly due to the oxidation of graphite.

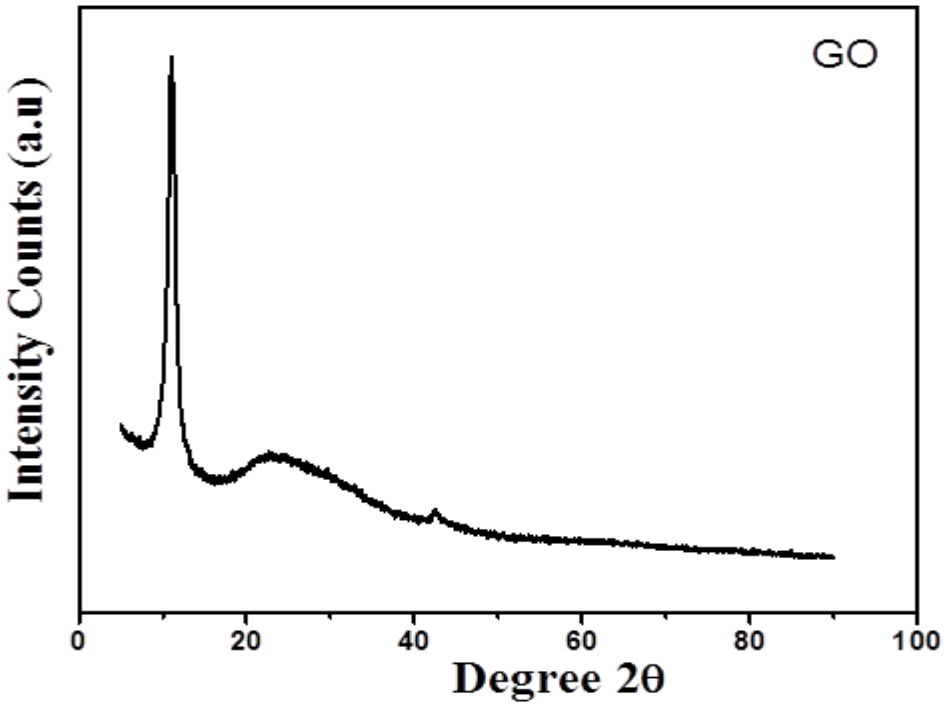


Figure 24: XRD of Graphene Oxide

An XRD graph is plotted for RGO/PVDF/Fe, PVDF, PVDF/Fe and Fe to show the difference in generation of peaks at various positions which are generated because of the presence of different molecules in the composite. These peaks are matched with the observed peaks in various published research papers. The figure also has helped us to observe the different phases of PVDF. The formation of crystalline polar γ-phase in the Fe-RGO/PVDF composite is confirmed by XRD analysis. As observed in by XRD analysis, several characteristic diffraction peaks of only PVDF are observed at 2θ of ≈ 17.6, ≈18.3, ≈ 19.9 and ≈ 26.5º these are the corresponding reflection planes of (100), (020), (110) and (021) respectively, attributing to non-polar α-phase polymorph. Also, a peak is seen at a 2θ ≈ 20.1º in RGO/PVDF/Fe composite that corresponds to the diffraction from (002) plane. This peak is an indication for the stabilization of polar γ-crystalline phase of the PVDF in the composite. It is possibly attributed to either α- or β – or γ-phase, i.e., very close to each other and is complicate to distinguish from each other by XRD analysis.

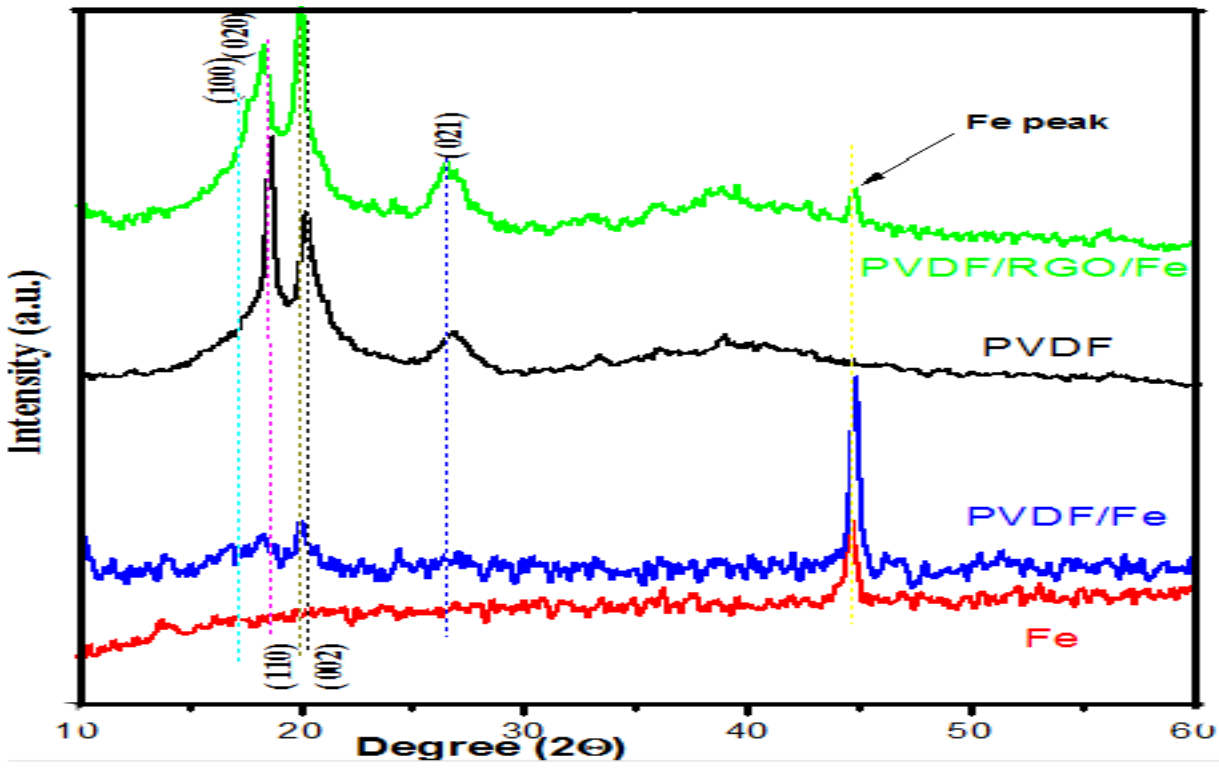


Figure 25: XRD of various film of (top to bottom) RGO/PVDF/Fe, PVDF, PVDF/Fe and Fe

### 5.2 FTIR Analysis

FTIR spectroscopy is a very powerful technique to study the molecular orientation and ordering. The Infrared (IR) spectroscopy detects vibration characteristics of the chemical functional group in a sample.

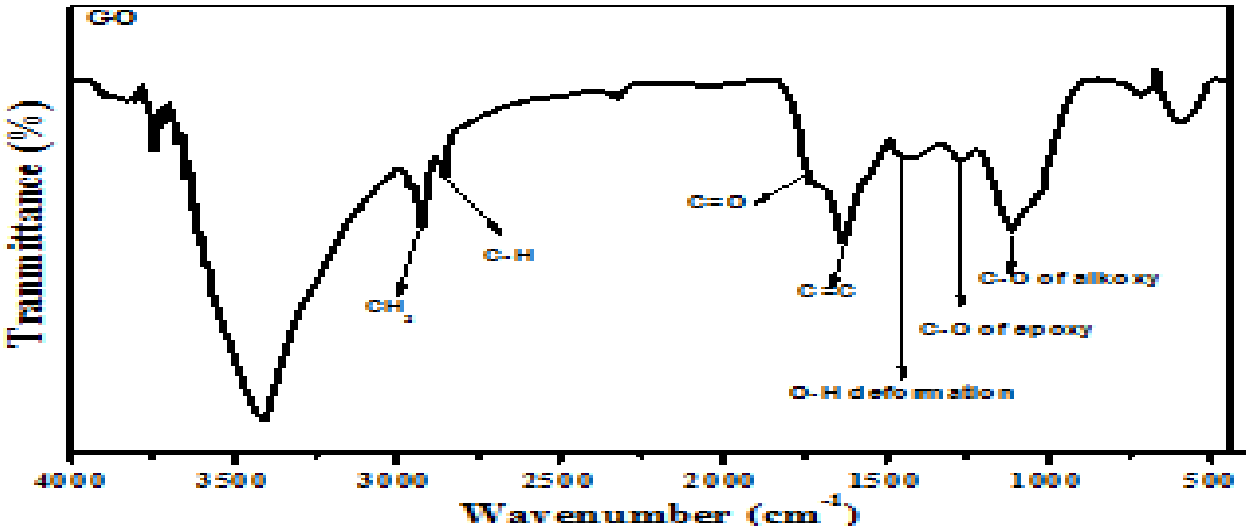


Figure 26: FTIR of Graphene Oxide

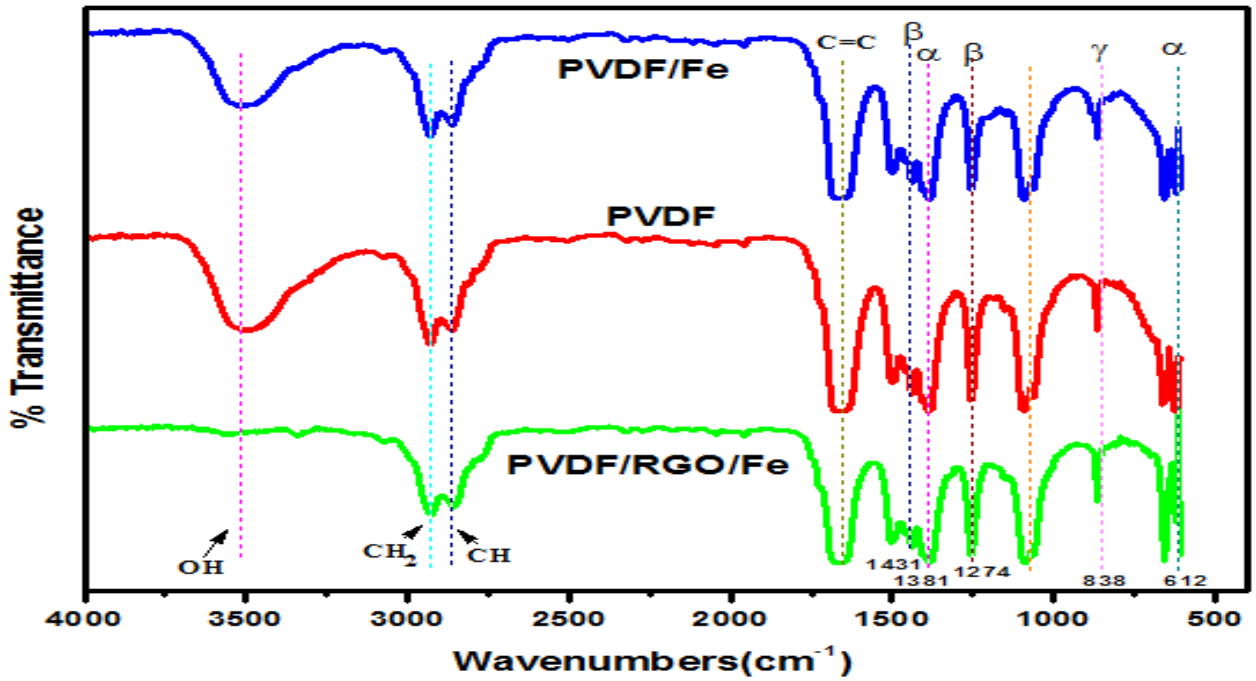


Figure 27: FTIR of films of (top to bottom) PVDF/Fe, PVDF, RGO/PVDF/Fe

The FTIR figure shows the various peaks generated. FT-IR spectroscopy gives the detail idea about the exact phase formation of the RGO/PVDF/Fe composite, PVDF and PVDF/Fe composite. The characteristics absorption bands of non-polar α, polar β and γ-phases of neat PVDF, PVDF/Fe and RGO/PVDF/Fe composites are observed at 612, 1210, 1381 and 1423 $cm^{-1}$ for α- phase; 510, 840, 1274, 1286, 1431 $cm^{-1}$ for β-phase and 812, 833, 838 and 1233 $cm^{-1}$ for γ-phase. But, in most of the cases, absorption bands of β and γ-phases PVDF are superimposed due to common TTT confirmations which create difficulty in phase separation among them.

The first curve of PVDF/Fe shows a large peak at 3500 $cm^{-1}$ , which may be due to OH bond in water present as impurity. Also peaks at 2929$cm^{-1}$ and 2859 are seen which may be due to presence of $CH_2$ and CH bonds present in PVDF. Also, peaks at 1381$cm^{-1}$ and 612 $cm^{-1}$ are obtained due to the presence of non-polar α phase present in PVDF and the peaks at1431$cm^{-1}$ and 1274$cm^{-1}$ can be observed because of polar β phase of PVDF. Also, a single peak at 838$cm^{-1}$ is seen because of γ phase of PVDF.

From the FTIR it can be observed that most of the peaks because of PVDF only this could be because of the presence of PVDF in large quantity, which may have surrounded other elements present in the composite.

### 5.3 SEM analysis

The morphology of the composite was investigated with the Scanning Electron Microscopy. Figure (a) and figure (b) show graphene oxide's smooth layers stacked one above the other whereas figure (c) and (d), show PVDF polymer completely covering the RGO, and there is an increase in the roughness.

Figure (e) shows the interface of PVDF and Fe layer and figure (f) shows the magnified PVDF polymer part in the composite made of PVDF and Fe using water.

Figure (g) and (h) show the PVDF and Fe composite and figure (i) ad (j) show the PVDG/RGO/Fe composite where an increase in the roughness can be clearly observed because of high quantity of Fe present in the composite.

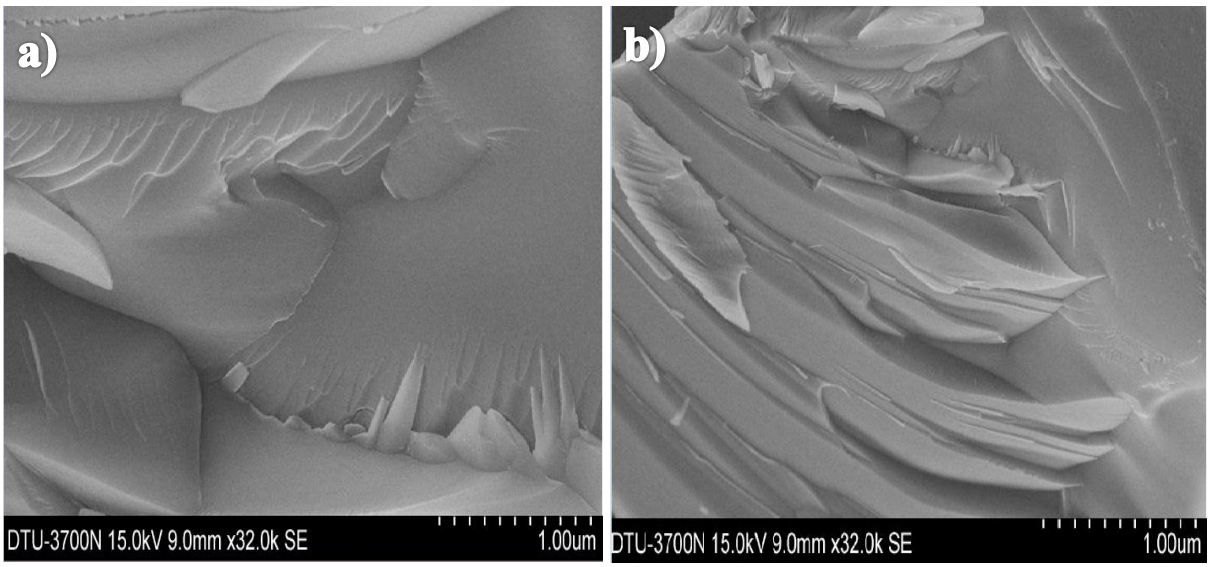


Figure 28: (a) and (b) show SEM image of Graphene oxide

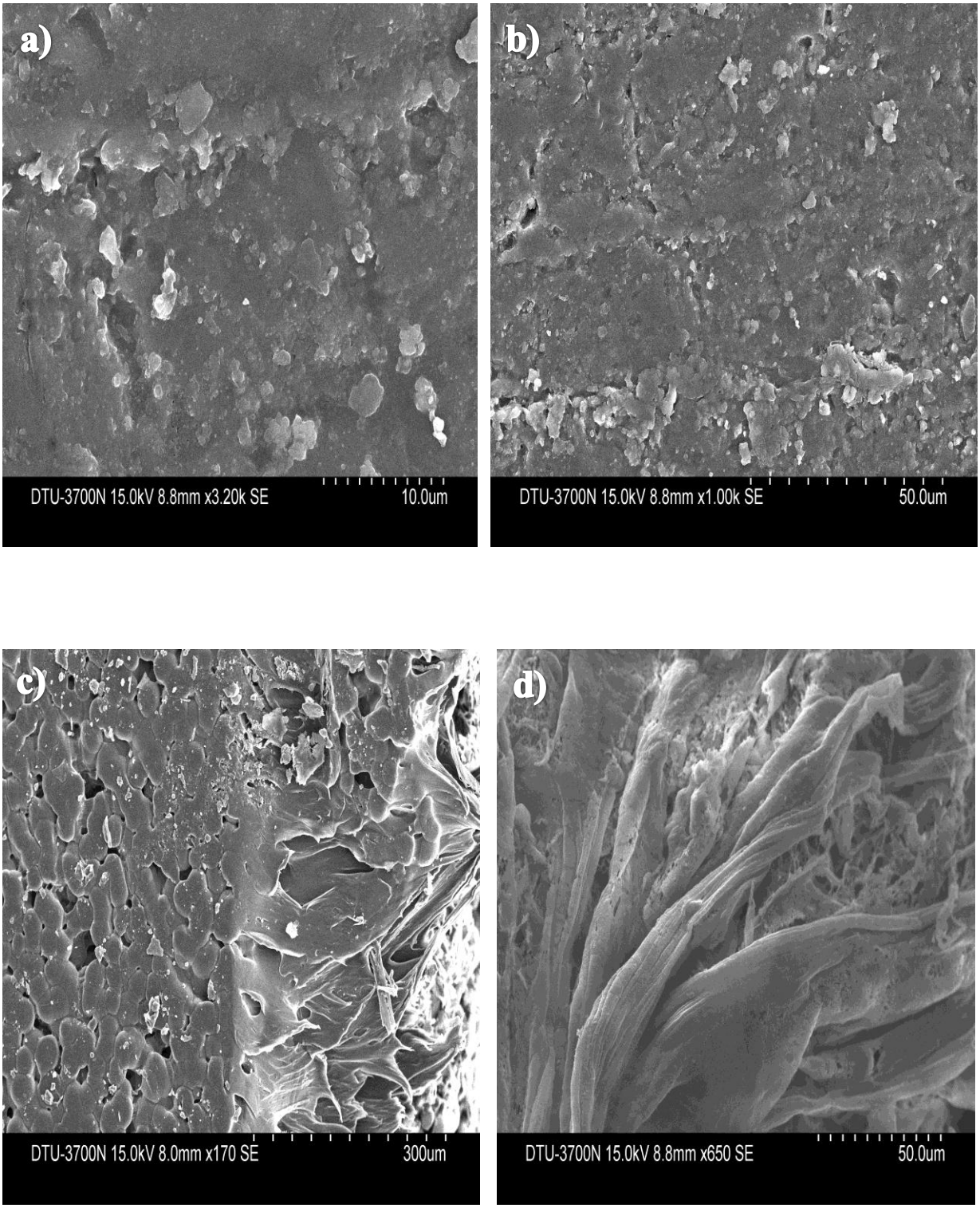


Figure 29: (a) and (b) show SEM image of RGO/PVDF, (c) and (d) show SEM images of PVDF/Fe and PVDF film respectively using water

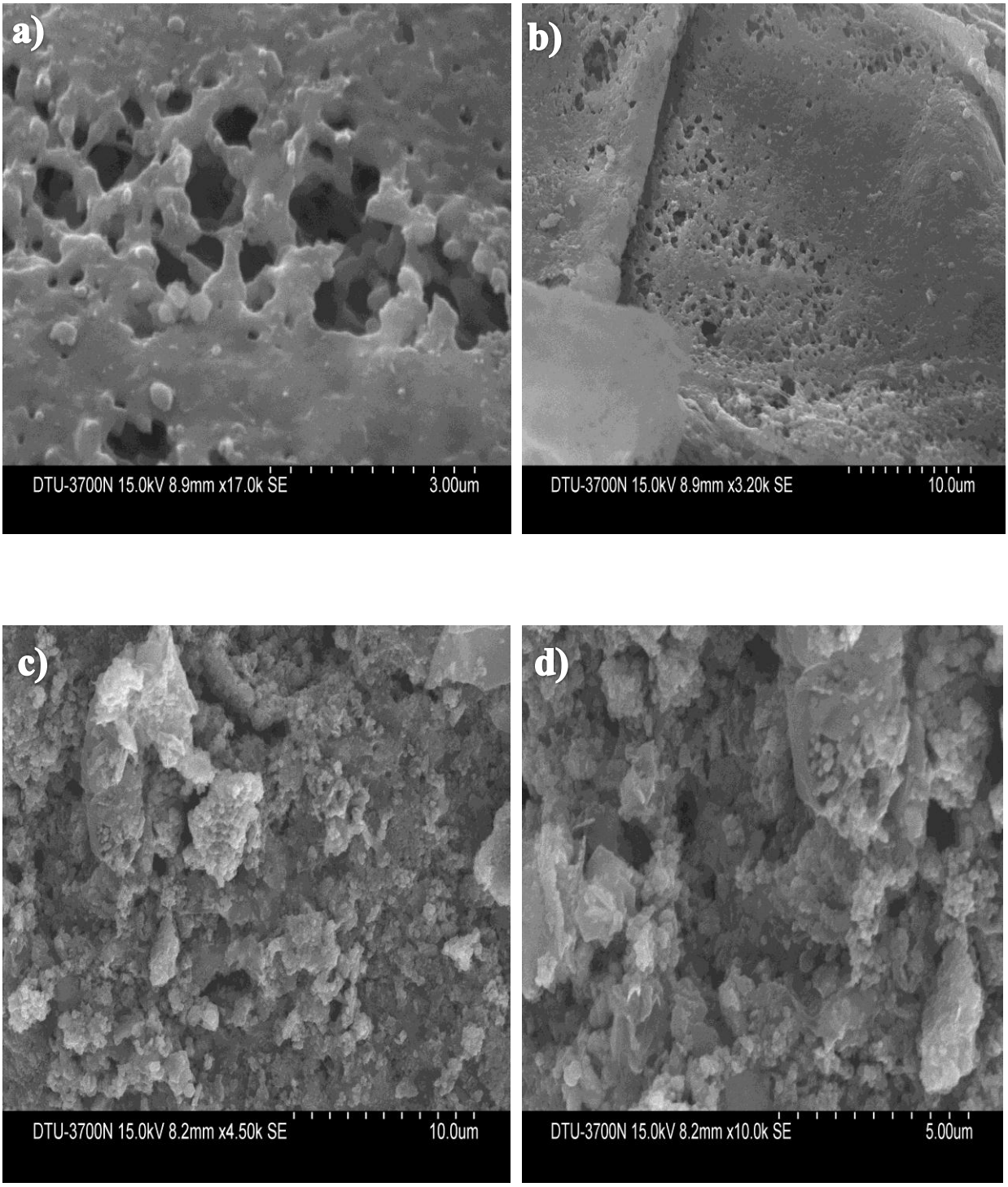


Figure 30: (a) and (b) show SEM image of RGO/PVDF film, (c) and (d) show SEM image of RGO/PVDF/Fe film

### 5.4 EDX

The chemical composition of graphene oxide prepared, was extracted from the energy dispersive X-ray spectrum (EDX). The EDX analysis exhibited peaks of only C and O elements, and no additional peaks were detected, which means that GO prepared is exempted from impurities that arise while preparing the material. The atomic percentage of C and O elements present in the as prepared GO are 86.19% and 13.81% respectively.

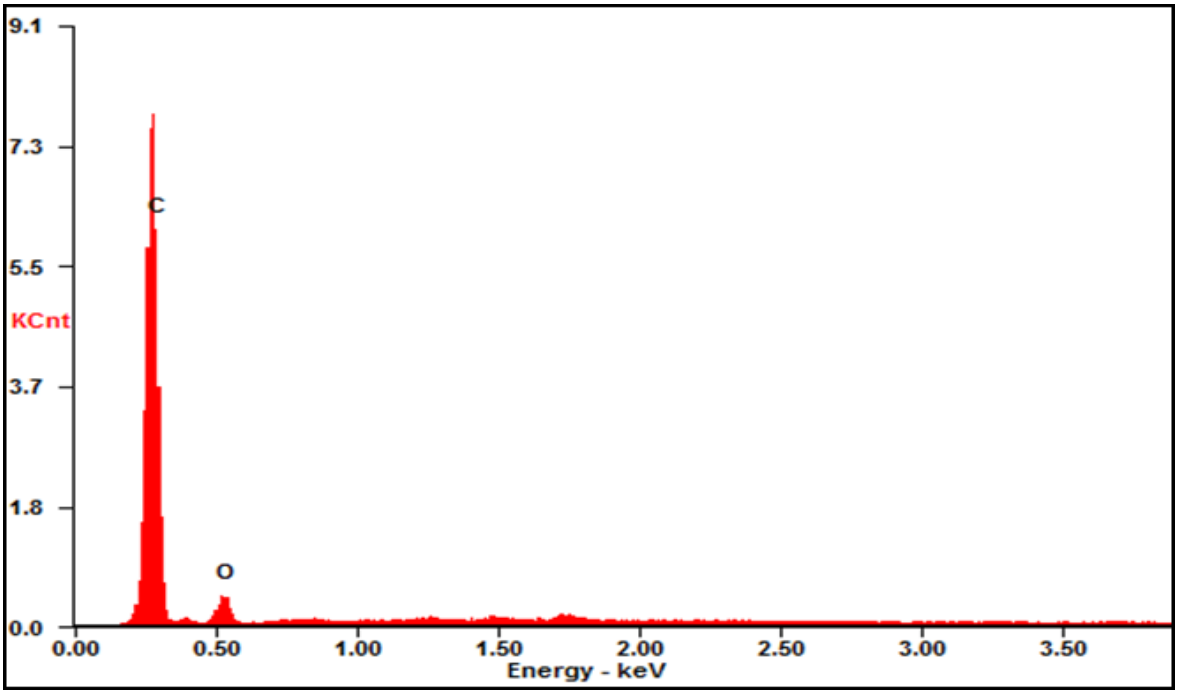


| Element | Wt% | At% |
|---|---|---|
| CK | 82.41 | 86.19 |
| OK | 17.59 | 13.81 |

Figure 31: EDX analysis of Graphene Oxide

## 5.5 TEM

In order to study detailed information about GO, TEM was used. Figure (a) clearly shows wrinkling and overlapping of graphene oxide layers over each other. Figure (b) shows a highly magnified image of GO.

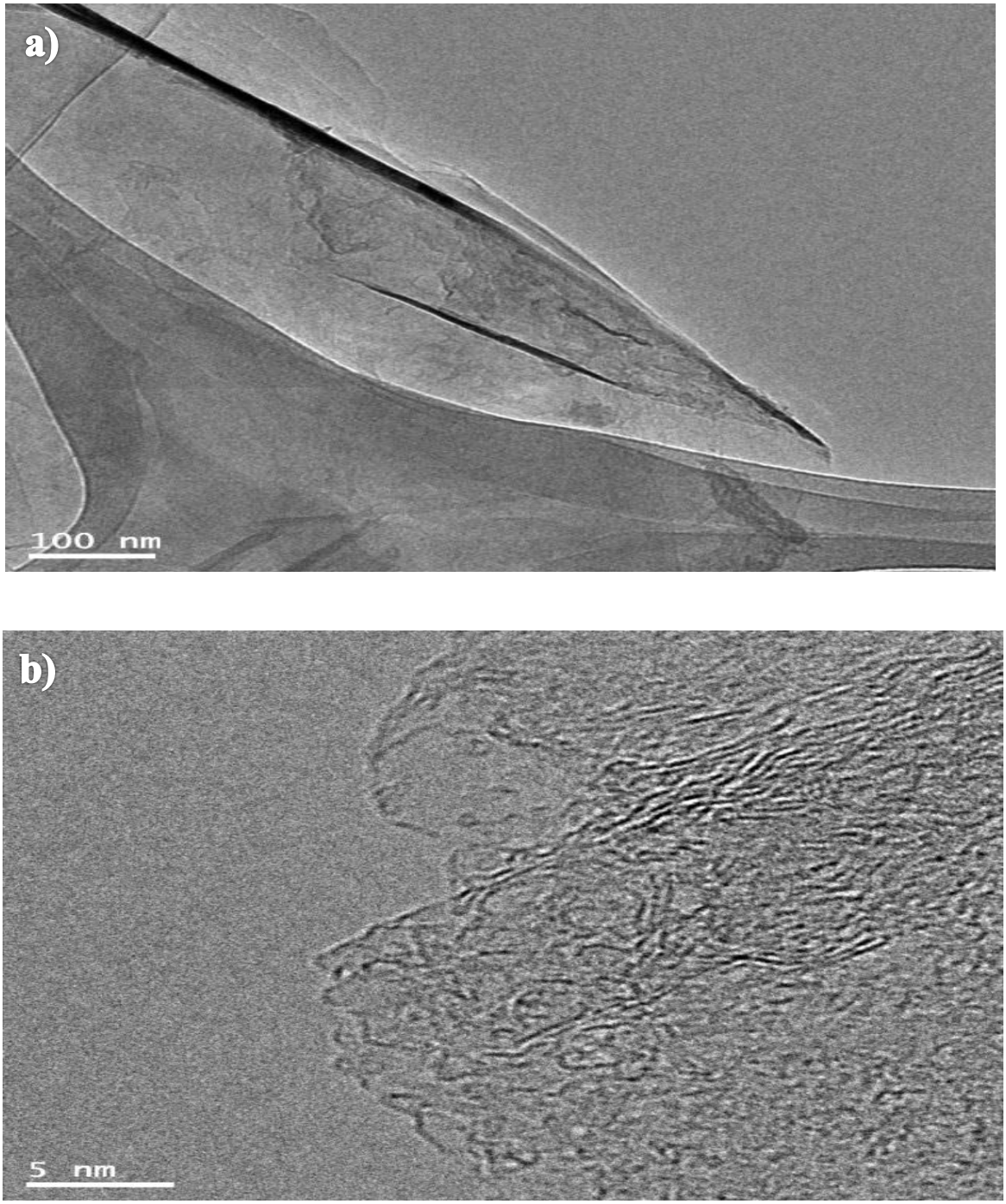


Figure 32: (a) and (b) show TEM image of Graphene Oxide

### 5.6 Burn test observations

From the table it can be concluded that as the amount of filler content Fe is increased there s a decrease in the burning rate, this may be because Fe is a metal and does not burn. Also, all the composites show a similar burning pattern. They burn creating white smoke and black ash and all are self-extinguishing. One Other thing that was observed during the bun test was that when GO alone was burnt, its burning rate was quite high and it burned creating sparks and was also non self-extinguishing but when a composite was made with PVDF then there was a huge change in its properties. This change may be due to the domination of PVDF over RGO, because of the use of PVDF in large quantity as compared to RGO.

| **Observations** | **Compounds** | | | |
|---|---|---|---|---|
| | **PVDF/ Fe $_{1g}$** | **PVDF/RGO $_{0.1g}$** | **PVDF/RGO$_{0.1}$/Fe$_{0.5g}$** | **PVDF /Fe $_{1g}$ (WATER)** |
| **Burn rate (cm/min)** | 0.41 | 0.50 | 0.46 | 0.52 |
| **Drips** | No | No | No | No |
| **White Smoke** | Yes | Yes | Yes | Yes |
| **Self-Extinguish** | Yes | Yes | Yes | Yes |
| **Ash** | Yes | Yes | Yes | Yes (but very less) |

Table 5.1 Burn test observations

## 5.7 Piezoelectric Energy harvesting property

### 5.7.1 CRO readings

It can be concluded from graph (a) that as the amount of Fe is increased (keeping the amount of PVDF and RGO constant), an increase in the amount of voltage generated is increased, which reaches up to a certain optimum level (i.e. Fe=0.5g) and then starts to decrease. The initial increase in the amount of voltage generated may be because Fe is highly conductive in nature, but after a certain quantity it starts hindering with the working of the PVDF.

The graph shows an optimum voltage generated of 0.74V but the highest voltage that was 0.93V which can be seen in the images of the multi-meter.

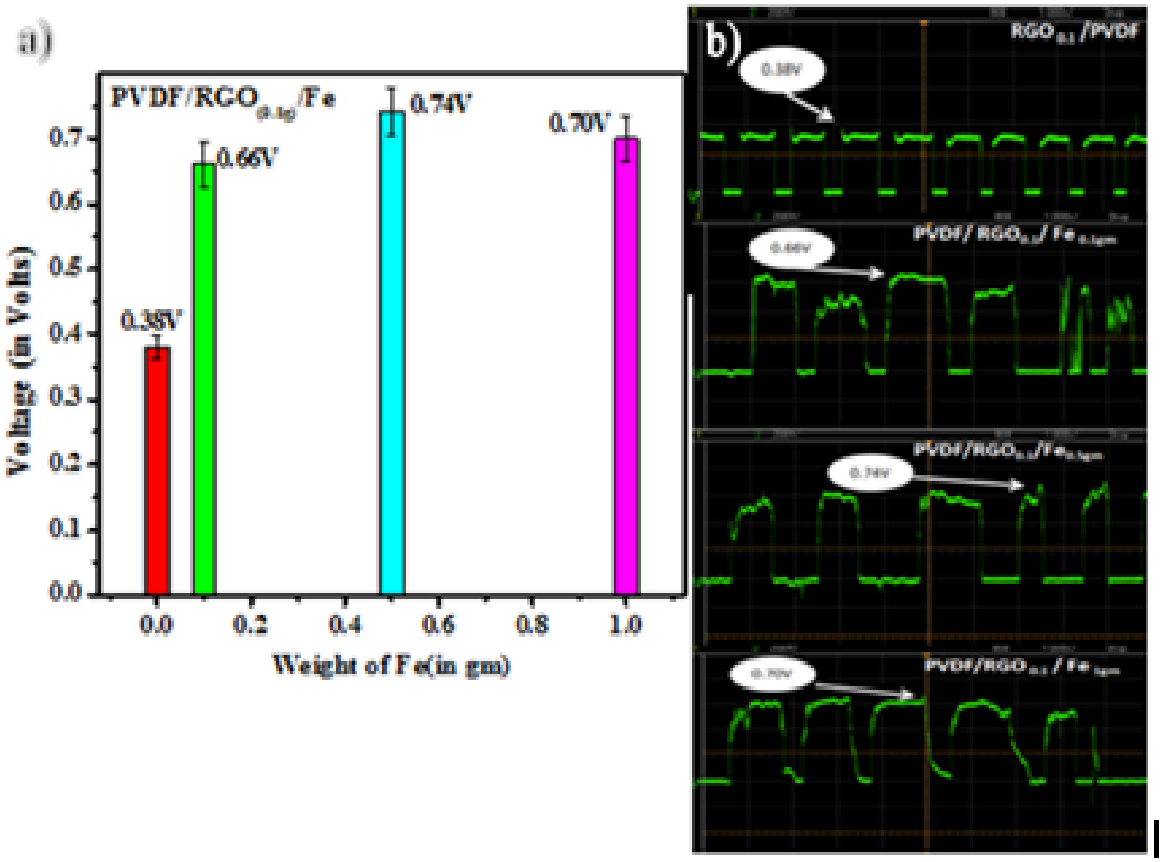


Figure 33: (a) Graph of peak voltages obtained from CRO (b) Images from CRO of response of films with varying Fe content in PVDF/RGO$_{(0.1g)}$/Fe due to external force

It can be concluded from graph (b) that as the amount of Fe is increased (keeping the amount of PVDF constant), an increase in the amount of voltage generated is increased, which reaches up to a certain optimum level (i.e. Fe=1.0g) and then starts to decrease. The initial increase in the amount of voltage generated may be because Fe is highly conductive in nature, but after a certain quantity it starts hindering with the working of the PVDF.

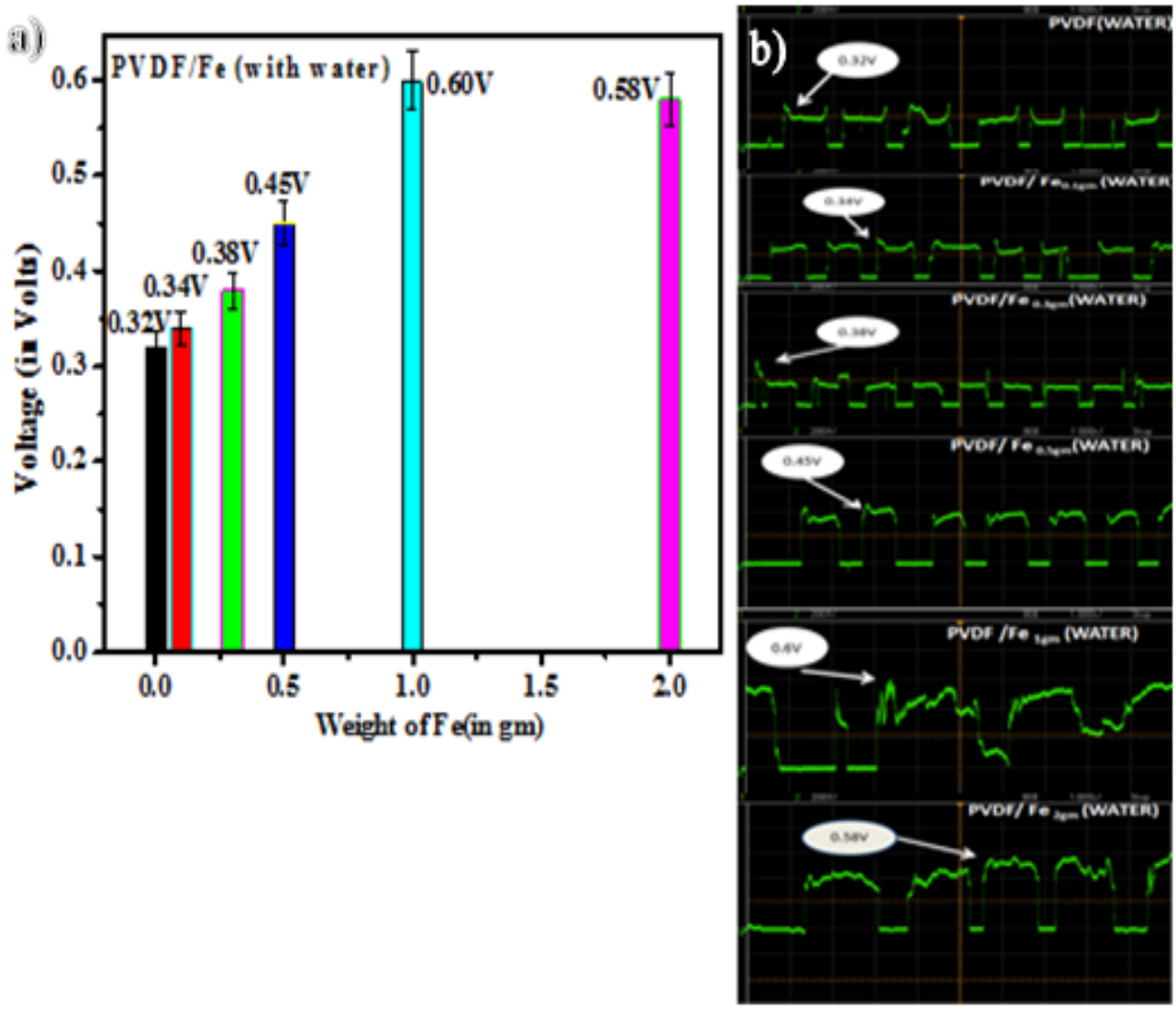


Figure 34: (a) Graph of peak voltages obtained from CRO (b) Images from CRO of response of films with varying Fe content in PVDF/Fe (WATER) due to external force

It can be concluded from graph (a) that as the amount of RGO is increased (keeping the amount of PVDF constant with no Fe content), an increase in the amount of voltage generated is increased, which reaches up to a certain optimum level (i.e. RGO=0.1g) and then does not increase i.e. remains same. The initial increase in the amount of voltage generated may be because RGO is more conductive in nature than PVDF, but after a certain quantity it starts hindering with the working of the PVDF.

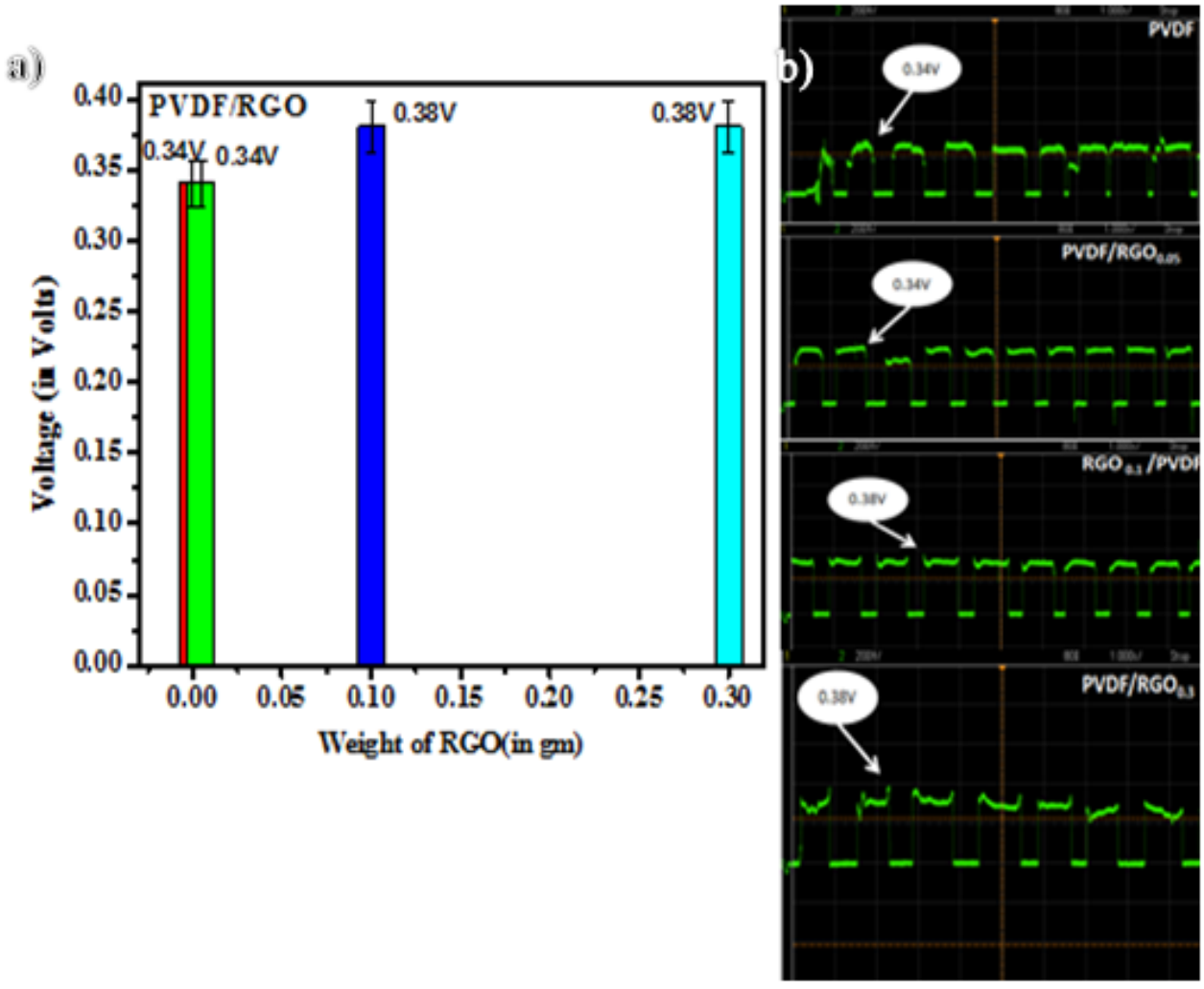


Figure 35: (a) Graph of peak voltages obtained from CRO (b) Images from CRO of response of films with varying RGO content in PVDF/RGO due to external force

It can be concluded from graph (a) that as the amount of Fe is increased (keeping the amount of PVDF constant and no RGO), an increase in the amount of voltage generated is increased, which reaches up to a certain optimum level (i.e. Fe=1.0g) and then starts to decrease. The initial increase in the amount of voltage generated may be because Fe is highly conductive in nature, but after a certain quantity it starts hindering with the working of the PVDF.

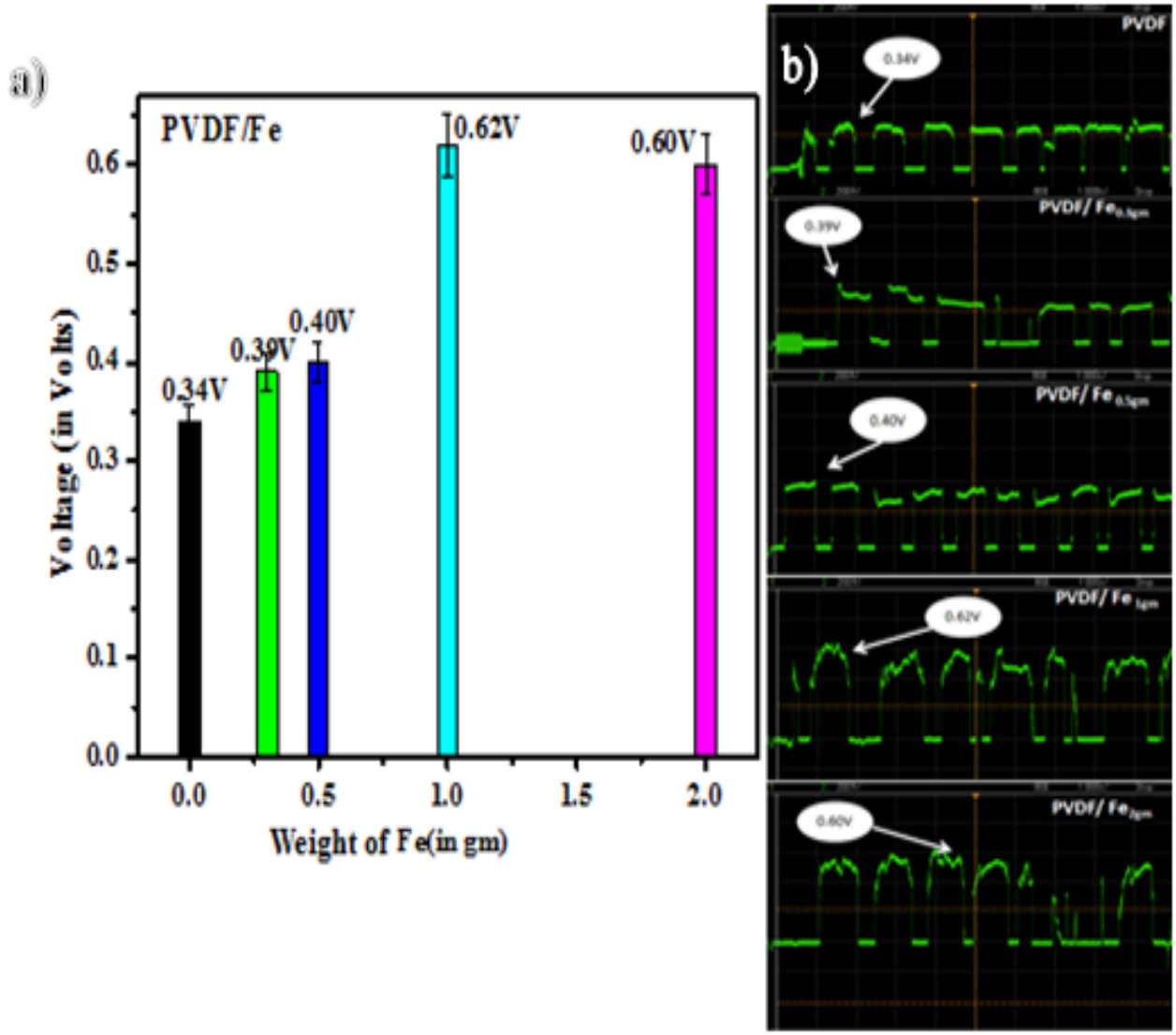


Figure 36: (a) Graph of peak voltages obtained from CRO (b) Images from CRO of response of films with varying Fe content in PVDF/Fe due to external force

### 5.7.2 Multimeter Readings

From the figure it can be seen that different composite film generate different amount of voltage. An Optimum amount of 0.93V can also be seen, this voltage was generated by PVDF/$RGO_{0.1}$/$Fe_{0.5g}$ when very high pressure was applied at a very high change of rate.

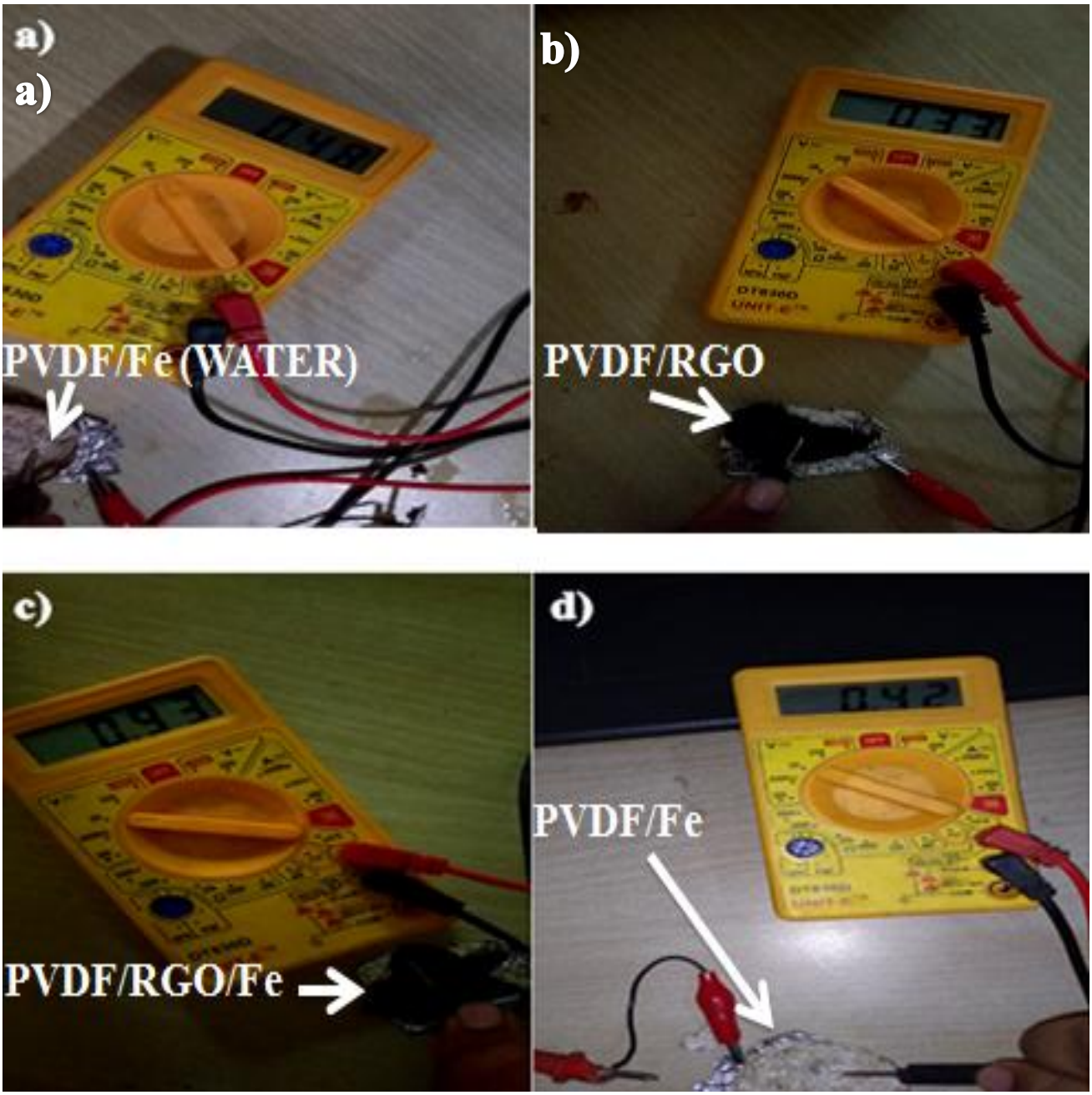


Figure 37: Images of output voltage generated from various composite films in a multimeter

### 5.2.8 Application of harvested energy

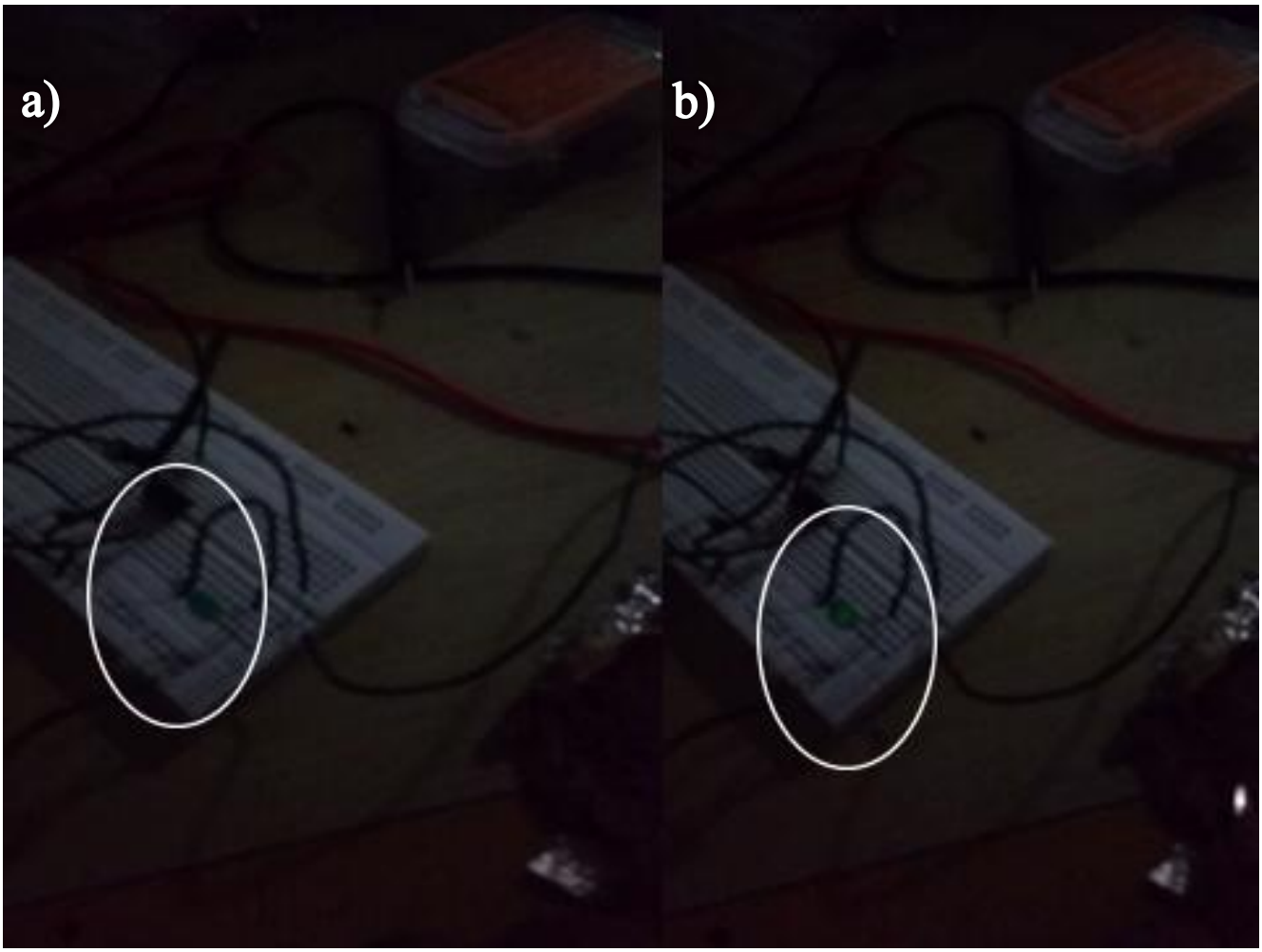


Figure 38: (a) Image of non-illuminated LED when film is not pressed, (b) Image of illuminated LED when film is pressed using charge amplifier

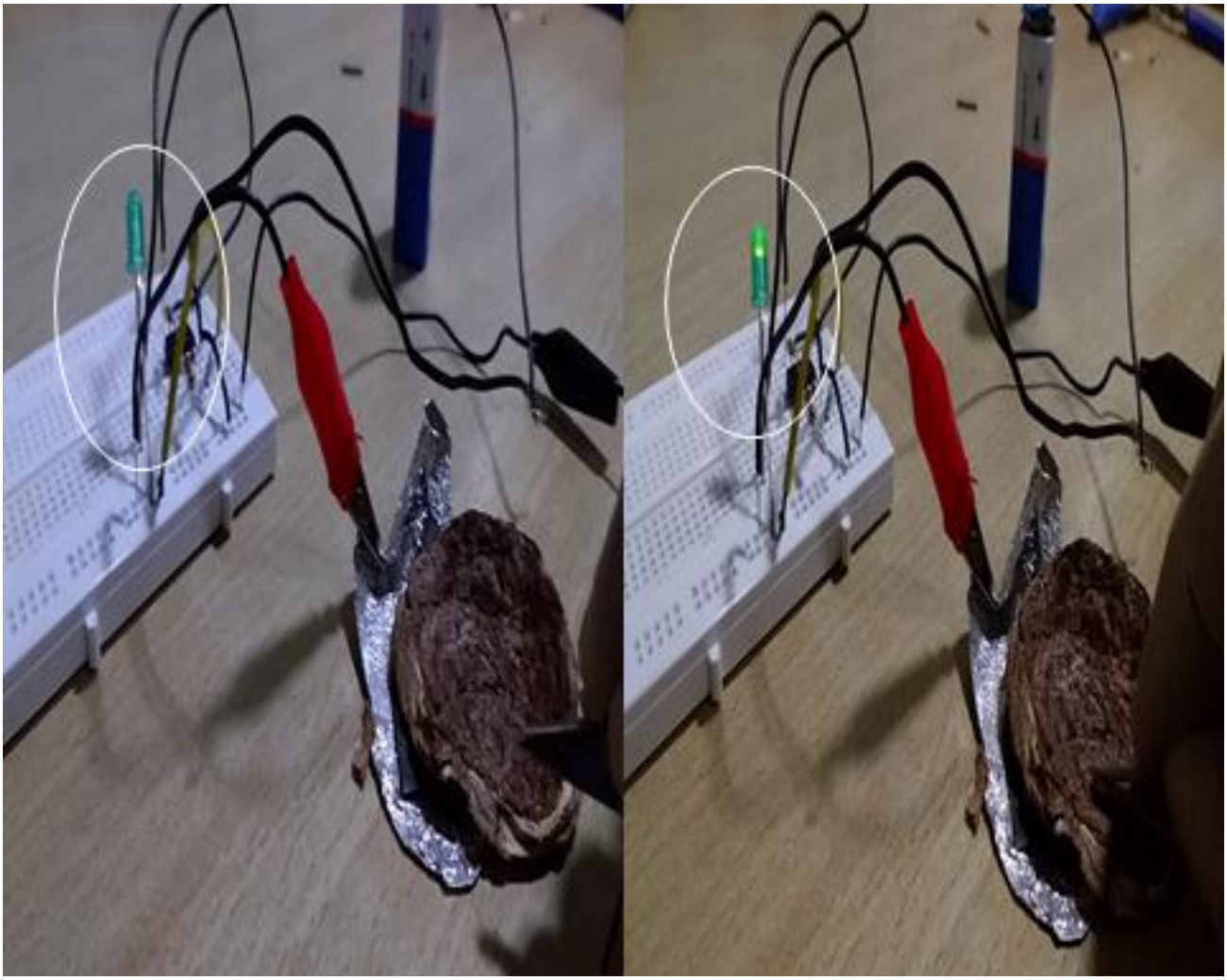

Figure 39: (a) Image of non-illuminated LED when film is not pressed, (b) Image of illuminated LED when film is pressed using circuit of voltage amplifier

# *CHAPTER 6*

# Conclusion

We developed a flexible piezoelectric energy harvesting devices with RGO/Fe nanosheet and PVDF polymer composite. By controlling the Fe and RGO concentration, an optimum amount of voltage i.e. 0.93V was generated which was the amplified using an electronic circuit to glow a LED. The composite shows that high level of finger touch sensitivity that possibly can be used in portable electric and electronic devices as pressure or touch senors. The high performance of the piezoelectric energy harvester provides us a new platform that could be used for scavenging energy from environment and we will be able to store the power using capacitors.

## Future Aspects

In the future more energy can be harvested using different piezoelectric, or their composite materials like quartz crystal, ceramics etc. The energy generated by the prepared composite can be used not only to glow LED but also in low power electronic devices like buzzers, earphones, pendrives, electronic circuits etc.

Also the energy generated from these films can be stored in capacitors which can further be used as a recharging battery or for charging mobiles etc. For powering medium power devices i.e. up to 15V, these films can be connected in series and when pressure is applied, a potential difference up to 12V to 15V can be easily generated.

Thus these films have a vast future scope and can solve the problem of our energy demand.

## References


1. Z. L. Wang and J. H. Song, Science, 2006, 312, 242–246.
2. Z. L. Wang and W. Wu, Angew. Chem., 2012, 51, 11700–11721.
3. V. Bhavanasi, D. Y. Kusuma and P. S. Lee, Adv. Energy Mater., 2014, 4,1400723–1400730.
4. B. Saravanakumar, S. Soyoon and S. J. Kim, ACS Appl. Mater. Interfaces, 2014, 6,13716–13723.
5. P. Martins, A. C. Lopes and S. L. Mendeza, Prog. Polym. Sci., 2014, 39, 683–706.
6. A. J. Lovinger, Science, 1983, 220, 1115–1121.
7. B. Saravanakumar, R. Mohan, K. Thiyagarajan and S. J. Kim, RSC Adv., 2013, 3, 16646–16656.
8. Z. H. Lin, Y. Yang, J. M. Wu, Y. Liu, F. Zhang and Z. L. Wang, J. Phys. Chem. Lett.,2012, 3, 3599–3604.
9. K. I. Park, C. K. Jeong, J. Ryu, G. T. Hwang and K. J. Lee, Adv. Energy Mater., 2013, 3,1539–1544.
10. 10 . M. M. Alam, S. K. Ghosh, A. Sultana and D. Mandal, Nanotechnology, 2015, 26,165403.
11. C. T. Huang, J. Song, W. F. Lee, Y. Ding, Z. Gao, Y. Hao, L. J. Chen and Z. L. Wang, J. Am. Chem. Soc., 2010, 132, 4766–4771.
12. M. L. Seol, J.-H. Woo, D.-I. Lee, H. Im, J. Hur, and Y. K. Choi, Small, 2014, 10, 103887–3894.
13. .Z. L. Wang, Faraday Discuss., 2014, DOI: 10.1039/c4fd00159a.
14. H. Kawai, Jpn. J. Appl. Phys. 1969, 8, 975–976.
15. J. Wang, H. Li, J. Liu, Y. Duan, S. Jiang and S. Yan, J. Am. Chem. Soc., 2003, 125,1496–1497.
16. N. Levi, R. Czerw, S. Xing, D. Iyer and D. L. Carroll, Nano Lett., 2004, 4, 1267–1271.
17. C. C. Hong, S. Y. Huang, J. Shieh and S. H. Chen, Macromolecules, 2012, 45, 1580–1586.
18. W. Li, Q. Meng, Y. Zheng, Z. Zhang and W. Xia, Appl. Phys. Lett., 2010, 96, 192905–908.
19. Q. M. Zhang, V. Bharti and X. Zhao, Science, 1998, 280, 2101–2104.

20. M. Li, H. J. Wondergem, M. J. Spijkman, K. Asadi, I. Katsouras, P. W. M. Blom and D. M. de Leeuw, Nat. Mater., 2013, 12, 433–439.
21. M. C. G. Gutierrez, A. Linares, J. J. Hernandez, D. R. Rueda, T. A. Ezquerra, P. Poza and R. J. Davies, Nano Lett., 2010, 10, 1472–1476.
22. M. Li, N. Stingelin, J. J. Michels, M. J. Spijkman, K. Asadi, K. Feldman, P. W. M. Blom and D. M. Leeuw, Macromolecules, 2012, 45, 7477–7485.
23. Alamusi, J. M. Xue, L. K. Wu, N. Hu, J. Qiu, C. Chang, S. Atobe, H. Fukunaga, T. Watanabe, Y. L. Liu, H. M. Ning, J. H. Li, Y. Lif and Y. Zhaog, Nanoscale, 2012, 4, 7250–7255.
24. G. H. Kim, S. M. Hong and Y. Seo, Phys. Chem. Chem. Phys., 2009, 11, 11506–11512.
25. Y. Li, J. Z. Xu, L. Zhu, H. Xu, M.-W. Pan, G. J. Zhong and Z. M. Li, Polymer, 2014, 55, 4765–4775.
26. X. J. Zhang, G. S. Wang, Y. Z. Wei, L. Guo and M. S. Cao, J. Mater. Chem. A., 2013, 1, 12115–12122.
27. . A. C. Lopes, C. M. Costa, C. J. Tavares, I. C. Neves, and S. Lanceros-Mendez, J. Phys. Chem. C, 2011, 115, 18076–18082.
28. B. Jaleh and A. Jabbari, Appl. Surf. Sci., 2014, 320, 339–347.
29. R. K. Layek, S. Samanta, D. P. Chatterjee and A. K. Nandi, Polymer. 2010, 51, 5846–5855.
30. P. Martins, C. M. Costa, M. Benelmekki, G. Botelho and S. Lanceros-Mendez, J. Mater. Sci., 2013, 48, 2681–2689.
31. A. K. Geim, Science, 2009, 324, 1530–1534.
32. Z. Li, X. Zhang, and G. Li, Phys. Chem. Chem. Phys., 2014, 16, 5475–5479.
33. S. K. Ghosh, M. M. Alam and D. Mandal, RSC Adv., 2014, 4, 41886−41894.
34. M. Kanik, O. Aktas, H. S. Sen, E. Durgun and M. Bayindir, Acs Nano, 2014, 8,9311–9323.
35. D. Mandal, K. Henkel, and D. Schmeisser, J. Phys. Chem. B, 2011, 115, 10567–10569.
36. Y. Li, J. Z. Xu, L. Zhu, G. J. Zhong and M. Li, J. Phys.Chem.B, 2012,116,14951−14960.
37. Y. Li, J.Z.Xu, L.Zhu, G. J. Zhong and Z.M.Li, J.Phys.Chem.B, 2012, 116,14951−14960.
38. P.C.A. Hammes, P.P.L. Regtien, An integrated infrared sensor using the pyroelectric polymer PVDF, Sens. Actuators, A 32 _1992.396–402.

39. Balaprasad, Farah (2012) Water soluble graphene synthesis.10 500-507.
40. Benjamin (2011) Growing graphene via chemical vapour deposition.
41. http://arxiv.org/ftp/arxiv/papers/1212/1212.6413.pdf
42. Geim AK, Novoselov KS (2007) The rise of grapheme. Nature materials 6: 183-191.
43. Sohan C (2012) Bulk synthesis of Graphene Nanosheets.
44. Ling S, Bunshi F (2000) Massive production of graphene oxide from expanded graphite.